

Mesoscopic architecture enhances communication across the Macaque connectome revealing structure-function correspondence in the brain

Anand Pathak,^{1,2} Shakti N. Menon,¹ and Sitabhra Sinha^{1,2}

¹*The Institute of Mathematical Sciences, CIT Campus, Taramani, Chennai 600113, India*

²*Homi Bhabha National Institute, Anushaktinagar, Mumbai 400 094, India*

(Dated: July 30, 2020)

Analyzing the brain in terms of organizational structures at intermediate scales provides an approach to negotiate the complexity arising from interactions between its large number of components. Focusing on a wiring diagram that spans the cortex, basal ganglia and thalamus of the Macaque brain, we provide a mesoscopic-level description of the topological architecture of one of the most well-studied mammalian connectomes. The robust modules we identify each comprise densely inter-connected cortical and sub-cortical areas that play complementary roles in executing specific cognitive functions. We find that physical proximity between areas is insufficient to explain the modular organization, as similar mesoscopic structures can be obtained even after factoring out the effect of distance constraints on the connectivity. We observe that the distribution profile of brain areas, classified in terms of their intra- and inter-modular connectivity, is conserved across the principal cortical subdivisions, as well as, sub-cortical structures. In particular provincial hubs, which have significantly higher number of connections with members of their module, but relatively less well-connected to other modules, are the only class that exhibits homophily, i.e., a discernible preference to connect to each other. By considering a process of diffusive propagation we demonstrate that this architecture, instead of localizing the activity, facilitates rapid communication across the connectome. By supplementing the topological information about the Macaque connectome with physical locations, volumes and functions of the constituent areas and analyzing this augmented dataset, we reveal a counter-intuitive role played by the modular architecture of the brain in promoting global interaction.

I. INTRODUCTION

Cortical localization, which refers to specific regions of the cerebral cortex being associated with distinct functions such as vision and language, has long been a dominant paradigm in neuroscience [1]. As the connectome provides the physical substrate for cognition and behavior [2], it would seem intuitive that such localization would be reflected in the structural attributes of the network [3]. However, brain imaging studies show that a large number of regions become active during any cognitive task, ruling out a simple one-to-one correspondence between a certain set of vertices of the connectome and a particular function [4]. This suggests the necessity for a theoretic framework that investigates the dynamics of the brain in terms of how different areas connect and interact with each other [5]. Such an approach should integrate complementary perspectives that focus on (a) dynamics, where *distributed* activation of the entire network converges to different attractors, and (b) computation, in which *localized* processing of information occurs in a sequential manner, allowing us to interpret cognitive processing as dynamical computation [6].

An integrated view of how local and global coordination of activity across the brain can arise may be obtained by adopting a mesoscopic approach to analyzing the connectome. Such an approach focuses on understanding the interactions within and between communities of densely inter-connected brain areas (*modules*) that have been identified in nervous systems of different organisms [7–16]. Such structural modularity of the brain is expected

from the advantages that such an architecture may confer during evolution and development [15, 17], such as imparting robustness in the presence of constraints on wiring and performance [2, 18]. Traditionally, modules have been viewed in functional terms, associated with innate, domain-specific mental faculties (such as language) that are believed to be relatively independent of each other [19]. Examining how such cognitive modules relate to the structural communities of the connectome addresses the fundamental issue of structure-function correspondence in the brain [20, 21].

In this paper, we focus on the structure-function relation as evident in the modular organization of the Macaque connectome, which balances specialized and integrated processing by allowing rapid communication at both local and global scales. This is striking in view of the role that modularity plays in promoting information encapsulation in other network architectures [22]. In performing this analysis, we have added curated spatial and functional information concerning the brain areas to the existing database of brain connectivity, which can serve as a resource for the community. The modules revealed by our analysis extends earlier work [8, 12, 16] by including sub-cortical regions. We show that each module comprises both cortical and sub-cortical components, which is intriguing in view of the proposal that the thalamo-cortical loop plays a central role in the computational architecture of the neocortex [23]. More crucially, we show that the empirically determined pattern of intra- and inter-modular connectivity facilitates local, as well as global, dissemination, complementing studies showing

that maximizing information flow may cause model networks to evolve towards a modular structure [24, 25]. Furthermore, while it has been suggested earlier that physical space constraints cannot exclusively account for modules [10, 26, 27], our determination of the space-independent modules and their relatively high overlap with the original communities clearly indicate that the modularity of the Macaque brain has functional significance, viz., the facilitation of communication across the connectome.

II. MATERIALS AND METHODS

A. Data

Connectivity. We have used as the basis for reconstructing the Macaque connectome a directed network of brain regions (cortical and sub-cortical) that was compiled in Ref. [28] using several hundred tract tracing studies obtained from CoCoMac - a comprehensive neuroinformatics database [29–31]. The original network comprised 383 vertices, representing regions in the cortex, basal ganglia and thalamus, at different levels of spatial resolution, and 6602 directed edges corresponding to tracts, i.e., myelinated bundles of axons connecting different brain regions, which may span large distances. In this hierarchically organized arrangement of subdivisions starting from the level of the entire brain, the same region may occur multiple times as a vertex could represent an area that is part of a larger area corresponding to a different vertex. For example, the hippocampus is a vertex of the network, as are its subdivisions CA1, CA3 and Dentate Gyrus. Consequently, there is no unique mapping between brain regions and vertices of this network. It also leads to ambiguity in interpreting edges connecting vertices that occur at any of the levels other than the lowest one in the hierarchy. For instance, if both vertices A and B link to C, but B is a sub-division of A, it is unclear if the two edges are distinct. These issues make it difficult to interpret any results obtained by analyzing the original network.

In the connectome we consider here, these issues are avoided by considering only those nodes that occur at the lowest hierarchical level, i.e., corresponding to regions with no further sub-divisions, in the original network. This yields a network comprising 266 nodes, representing brain areas that span a range of spatial scales ranging from the visual cortex area V1 (which has a volume of $\sim 2000 \text{ mm}^3$) to the thalamic region PT#2 (which has a volume of less than 2 mm^3). The network that we consider, consequently, consists of the 2602 directed links that occur between these nodes. Note that this procedure leads to the network having a largest connected component of 261 nodes (as the following five regions do not have any reported connections to the other areas at the lowest hierarchical level: PT#2, 6b-beta, 4a, 4b and Sub.Th). Despite the reduction

in the size of the network upon removal of the aforementioned redundancies, the resulting connectome has similar macroscopic properties as the original network, such as the exponential nature of the degree distribution (Fig. S1).

Spatial Positions. As the brain connectome is a spatially embedded network, it is important to consider geometric information such as physical locations and extent of the different brain regions, in addition to the connection topology. As the original network [28] did not contain any spatial information, we have compiled a comprehensive database of the positions of the areas corresponding to each of the nodes, as well as, the volumes spanned by them. We have obtained the stereotaxic coordinates of each brain region in our connectome from several sources. Information about 134 of the 266 regions included in the connectome has been obtained from the website [32] associated with the Paxinos Rhesus Monkey Atlas [33]. For the remaining regions, we manually curated the requisite data from the relevant research literature. The position of a region is identified with the approximate location of its center obtained from the online three-dimensional visualization platform in the website mentioned above. The volume spanned by a particular region was estimated by approximating the cross-sectional area occupied by the region in each of the coronal sections of the brain in which it appears and obtaining the sum of these areas weighted by the thickness of the sections measured along the rostral-caudal axis. Data file *connectome_nodes.xls* in the SI contains the 3-dimensional coordinates of, and the volumes covered by, each of the brain regions that we obtained through the above analysis. It also lists the references that were used to obtain the information about each region.

B. Modularity.

A prominent mesoscopic structural property associated with many networks that occur in nature is modular organization. Modules (or communities) are subnetworks that are characterized by a higher density of connections between the constituent nodes compared to that between nodes belonging to different modules [34]. One of the most well-known approaches for determining the modules of a network is to maximize a quantitative measure, Q , defined for a given modular partitioning of the network as, $Q = L^{-1} \sum_{i,j} B_{ij} \delta_{c_i c_j}$, where $B_{ij} = A_{ij} - (k_i^{\text{in}} k_j^{\text{out}} / L)$ are elements of the modularity matrix \mathbf{B} [35, 36]. The adjacency matrix \mathbf{A} ($A_{ij} = 1$, if a directed link exists from j to i , and 0, otherwise) specifies the connection topology of the network, while the number of incoming and outgoing connections of node i are indicated by the in-degree $k_i^{\text{in}} = \sum_j A_{ij}$ and out-degree $k_i^{\text{out}} = \sum_j A_{ji}$, respectively, with $L (= \sum_j k_j^{\text{in}} = \sum_j k_j^{\text{out}})$ being the total number of connections in the network. The Kronecker delta

function δ_{ij} yields 1 if the communities c_i and c_j to which nodes i and j belong respectively, are identical, and is 0 otherwise.

Spectral analysis and its refinement. In order to achieve an optimal partitioning of the network through the maximization of Q we have used the spectral method [36]. Here, we first bisect the network by assigning nodes to one of two communities according to the sign of the elements of the eigenvector corresponding to the largest positive eigenvalue of the symmetrized modularity matrix $\mathbf{B} + \mathbf{B}^T$. Subsequently we refine the partition by swapping the nodes between communities in order to achieve the highest possible value of Q . The above procedure is carried out recursively on each of the communities to further subdivide them until Q cannot be increased further [36]. This approach yields a maximum value of Q for a partitioning of the network into 5 modules with $Q_{\text{spectral}} = 0.485$.

Robustness of the partitioning. To ensure that the modular partitions of the network obtained using the deterministic spectral technique (described above) are not sensitively dependent on the specific method used for maximizing Q , we have used the stochastic simulated annealing approach to obtain an ensemble of 10^3 optimal partitions. The dissimilarity between the different partitions generated by each realization of the annealing technique reflects the extent of degeneracy (and hence, ambiguity) inherent in the modular decomposition of the network. Following Refs. [37, 38], for each realization of the simulated annealing approach we begin with an arbitrary partition of the network and iteratively change the modular composition by implementing one of three types of operations: (i) move a randomly chosen node to any other module including a newly created one, (ii) merge two randomly chosen modules and (iii) split a randomly chosen module into two parts so as to minimize the number of connections between the two parts. Any one of the possible operations (across all types) is chosen at each step with equal probability. The resulting partition associated with a change ΔQ in the modularity is accepted with a probability $\exp(-|\Delta Q|/T)$ if $\Delta Q < 0$ and $p = 1$ otherwise. Here, the parameter T , which is analogous to temperature, is decreased over time according to a specified cooling schedule. The process terminates when the number of successive failures at altering the modules exceeds a threshold value. While the Q values corresponding to the partitions obtained for different realization span a wide range, most of them cluster around that obtained from the spectral method, Q_{spectral} . We focus on the 291 partitions whose Q value deviates from Q_{spectral} by less than 3%. As shown in the SI, the modular membership of 70% of the nodes remain invariant across all of these partitions, and are in fact identical to that obtained from the spectral method, underlining the robustness of the modular decomposition. We have also used alternative methods of module identification that do

not rely on maximizing Q , viz., the Infomap method [39], and have obtained qualitatively similar results.

C. Classification of brain regions according to their role in the mesoscopic structural organization of the connectome.

The importance of a given region within the topological organization of the Macaque brain network is indicated by its connectivity within its own module (as defined above), as well as that across the entire brain, which is evident from its connections to regions belonging to other modules. These can be quantitatively measured by the metrics (i) the within module degree z -score (z) and (ii) the participation coefficient (P), respectively [40, 41]. To identify regions that have significantly more connections within their own module, we determine a within module degree z -score:

$$z_i = \frac{k_{c_i}^i - \langle k_{c_i}^j \rangle_{j \in c_i}}{\sqrt{\langle (k_{c_i}^j)^2 \rangle_{j \in c_i} - \langle k_{c_i}^j \rangle_{j \in c_i}^2}}, \quad (1)$$

where $k_{c_i}^i$ is the number of links between region i and other regions belonging to its module (c_i) and the average $\langle \dots \rangle_{j \in c}$ is taken over all regions in a module c . As in Ref. [10], nodes (regions) having $z > 0.7$ are identified as hubs, the remainder being classified as non-hubs.

In order to distinguish between brain regions in terms of their inter-modular connectivity we calculate the participation coefficient P_i of region i as:

$$P_i = 1 - \sum_{c=1}^m \left(\frac{k_c^i}{k^i} \right)^2, \quad (2)$$

where k_c^i is number of links that region i has with those regions belonging to module c and $k^i = \sum_c k_c^i$ is the total degree of the i -th node (region). A region whose connections are restricted within its own module has $P_i = 0$ while one whose links are uniformly distributed among the different modules has P_i closer to 1. Based upon the value of P_i , which provides a measure of how well a node (region) bridges different modules, the non-hub regions are classified as ultra-peripheral (R1, $p \leq 0.05$), peripheral (R2, $0.05 < p \leq 0.62$), satellite connectors (R3, $0.62 < p \leq 0.8$) and kinless nodes (R4, $p > 0.8$), while the hubs can be demarcated into provincial hubs (R5, $p \leq 0.3$), connector hubs (R6, $0.3 < p \leq 0.75$) and global hubs (R7, $p > 0.75$).

D. Degree- and modularity-preserved network randomization.

We construct an ensemble of 10^3 networks obtained by randomizing the empirical network preserving the in-degree and out-degree of each node (region) as well as the modular organization of the network [10]. Each network

is obtained by selecting directed connections, e.g., $i \rightarrow p$ and $j \rightarrow q$, such that the source nodes i, j belong to the same module A and target nodes p, q belong to the same module B (which could be same as A), and then rewire them so as to have $i \rightarrow q$ and $j \rightarrow p$. This procedure is repeated for 10^6 times for each realization of a randomized network. To randomize the network preserving the degree alone, we follow the same procedure as above with the difference that there is no constraint on the modular membership of the nodes.

E. Diffusive spreading model.

As the function of the connectome is to facilitate communication between the different brain regions, we investigate the role of the empirically observed pattern of intra- and inter-modular connections on the diffusion of information across the system. For this purpose, we consider discrete random walks that, starting from a given node on the network, proceeds at each time step from one node to a randomly chosen node that receives an outwardly directed link from the former. The rate at which spreading occurs in different parts of the system can be analyzed by obtaining the distribution of first passage times (FPTs) for a random walk to reach a target node starting from a source node. For this, we have measured the FPTs τ to all nodes that are visited by a walk initiated from a given node of the network. The process is repeated 10^3 times starting from each of the 266 nodes, with a walk terminating when either every node has been visited at least once or a node with no outgoing connections is reached. Separate distributions for intra-modular FPTs (τ^{intra}) and inter-modular FPTs (τ^{inter}) can be obtained by considering the source and target nodes to be in the same module or in different modules, respectively. For comparison, we also compute the distributions of FPTs τ_D and τ_{DM} for randomized surrogates in which either the degrees, or both the degrees and modular memberships, of the nodes are preserved, respectively. In each case, the distribution is averaged over 20 network realizations. The deviation of the empirical FPT distribution from those obtained from the randomized surrogates by averaging over multiple realizations is quantified in terms of a z -score measure defined as:

$$z = \frac{P_{\text{emp}}(\tau) - \langle P_{\text{rand}}(\tau) \rangle}{\sqrt{\langle P_{\text{rand}}(\tau)^2 \rangle - \langle P_{\text{rand}}(\tau) \rangle^2}}, \quad (3)$$

where $P_{\text{emp}}(\tau)$ and $P_{\text{rand}}(\tau)$ are the empirical and randomized surrogate FPT distributions, respectively.

F. Role of spatial geometry in the modular organization of the connectome.

The physical distance d_{ij} between two brain regions i and j , whose centers are indicated by the vectors \mathbf{x} and \mathbf{y} , respectively, has been measured in terms of the

Euclidean metric $d(\mathbf{x}, \mathbf{y})$ and scaled by the geometric mean of the radii r_i, r_j of the two regions (the radius of each region being estimated from its volume, see SI).

Space-independent partitioning of the network into communities. For networks whose nodes are embedded in a space associated with a metric, it can be argued that the network properties, such as modularity, could be a consequence of the constraints imposed by the underlying geometry. We therefore need to modify the method for determining the modular structure of a network outlined above, in order to take into account the role of the physical space in which the network is embedded. This is done by re-defining the modularity matrix \mathbf{B} in the definition of the quantity Q (given above), so that the expectation of a pair of nodes (i, j , say) being connected by chance in the null model incorporates the physical distance (d_{ij}) between the nodes. Thus, following Ref. [42], we re-define $B_{ij} = A_{ij} - (k_i^{\text{in}} k_j^{\text{out}} f(d_{ij})/L)$, where $f(d) = \Sigma_{d_{ij}=d} A_{ij} / (k_i^{\text{in}} k_j^{\text{out}})$ is referred to as the *deterrence function*. This function, which is estimated from empirical data for the network, contains information about how the physical distance between a pair of nodes modulates their connection probability. Note that if the communities in the network arise entirely because of spatial dependence, measuring Q taking into account the physical distance between nodes does not yield any modular structure. Moreover, comparing the space-independent modular decomposition of the network obtained using this technique with the communities determined using exclusively information about the connection topology (as described earlier), we can infer whether the observed modularity is primarily driven by physical distance constraints (see SI). The similarity between the communities obtained using the two methods is quantified using *normalized mutual information*.

Normalized mutual information. To quantify the similarity between two modular decompositions $\{c_i^A\}_{i=1}^{M_A}$ and $\{c_j^B\}_{j=1}^{M_B}$ resulting from different partitionings A and B of a network (that yield M_A and M_B modules, respectively) we have used the normalized mutual information [43]

$$I_{\text{norm}}(A, B) = \frac{2 \sum_i \sum_j P(c_i^A, c_j^B) \ln [P(c_i^A, c_j^B) / P(c_i^A) P(c_j^B)]}{-\sum_i P(c_i^A) \ln P(c_i^A) - \sum_j P(c_j^B) \ln P(c_j^B)}, \quad (4)$$

where $P(c_i^A)$ is the probability that a randomly chosen node lies in module c_i^A in partition A , $P(c_j^B)$ is the probability that a randomly chosen node lies in module c_j^B in partition B , and $P(c_i^A, c_j^B)$ is the joint probability that a randomly chosen node belongs to module c_i^A in partition A , as well as, to module c_j^B in partition B ($i = 1, \dots, M_A$, and $j = 1, \dots, M_B$). Each of the probabilities can be estimated from the ratio of the community sizes to the size of the entire network.

Surrogate networks. In order to explicitly show that the

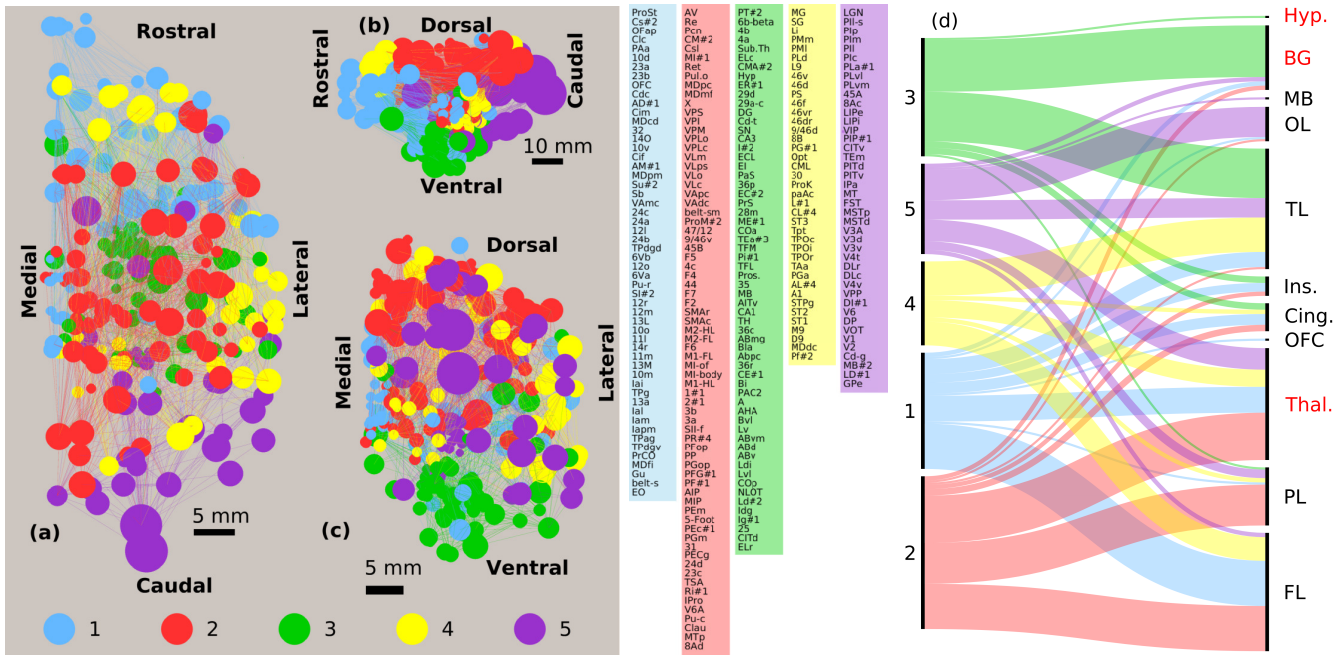


FIG. 1. **Mesoscopic organization of the Macaque brain.** The network of brain regions, shown in (a) horizontal, (b) sagittal and (c) coronal projections, clearly indicate that the nodes (filled circles) are organized into five modules, each characterized by dense intra-connectivity. The modular membership of each node is represented by its color (see color key to the right, containing the list of brain regions in each module), while node sizes provide a representation of the relative volumes of the corresponding brain regions (the spatial scale being indicated by the horizontal bar in each panel). The spatial positions of the nodes are specified by the three-dimensional stereotaxic coordinates of the corresponding regions (see Methods). Links indicate the directed nerve tracts connecting pairs of brain regions, and are colored in accordance with their source nodes. For details of each of the brain regions see SI. (d) Visual representation of the association between the network modules and cortical (in black), as well as, sub-cortical (in red) subdivisions of the brain, viz., *FL*: Frontal Lobe, *PL*: Parietal Lobe, *TL*: Temporal Lobe, *OL*: Occipital Lobe, *Cing.*: Cingulate, *Ins.*: Insula, *BG*: Basal Ganglia, *Thal.*: Thalamus, *Hyp.*: Hypothalamus, *OFC*: Olfactory complex, and *MB*: Mid-brain. For a detailed breakdown of the major subdivisions of the brain in terms of their module membership, see SI. This alluvial diagram has been created using the online visualization tool RAW [44].

modular organization is not primarily driven by the constraints imposed by the physical distance d between brain regions, we have demonstrated how spatial embedding affects the modular decomposition of a network, using three classes of surrogate random network ensembles (of size 100 each) having different underlying spatial dependences. The three ensembles, in increasing order of importance of d in governing the connection probability P between nodes, comprise networks with (a) $P \sim d^0$, (b) $P \sim d^{-1}$, which is the case in the empirical network, and (c) $P \sim \exp(-d)$, with nodes in each network occupying the same spatial position as in the empirical network. Each network (comprising an identical number of nodes and links as in the empirical network) was subject to community detection using information about the connection topology alone, as well as, space-independent modular decomposition, following the two approaches described above. The difference between these two sets of partitions provides a measure of the role that spatial embeddedness of the networks plays in determining the modular nature of their connectivity (see SI).

III. RESULTS

A. Mesoscopic organization of brain areas in the Macaque

Fig. 1 (a-c) shows the modular organization of the Macaque brain network spanning regions from the cortex, basal ganglia and thalamus, revealed by our analysis (for details see methods). The network is seen to comprise 5 modules, each module i being composed of m_i densely inter-connected brain regions (their numbers ranging between 39 and 71, see the color key to the right of Fig. 1, a-c, containing the list of brain regions in each module). The membership of the individual regions in these modules is seen to be robust (see Methods). Given that the network is embedded in a specific geometry, namely that of the Macaque brain, it is noteworthy that each of the modules are spatially clustered as is clearly seen from the projections shown in Fig. 1(a-c). To understand the implications of the spatial location of these modules, we visually represent the mapping between the modules and the major anatomical subdivisions of the brain in Fig. 1 (d) [see also SI].

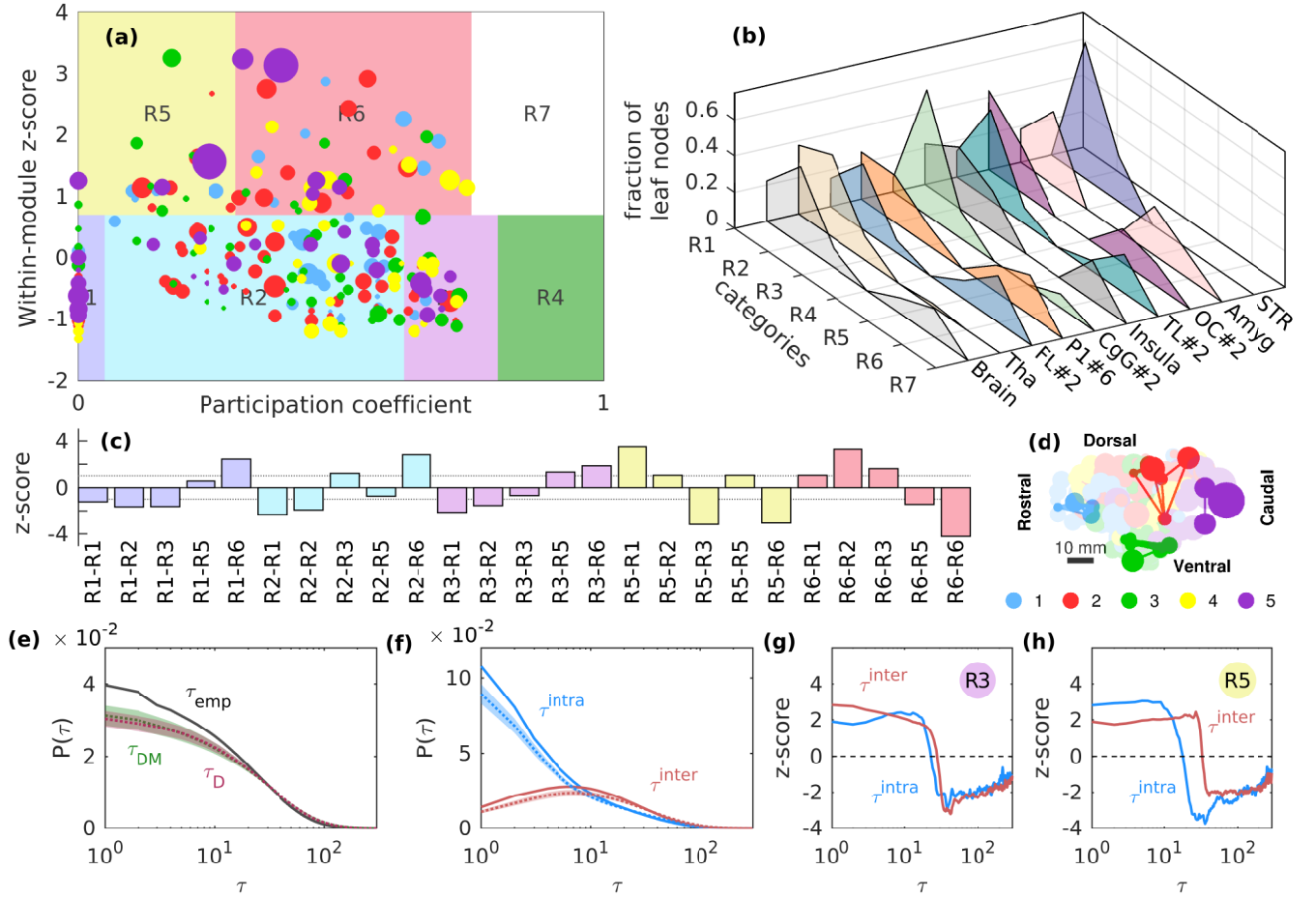


FIG. 2. Classification of brain regions according to their intra- and inter-modular connectivity. (a) Nodes of the Macaque brain network [colored and scaled as per Fig. 1 (a-c)] are displayed in accordance with their within-module degree z-score (z) and participation coefficient (P), which provide a measure of their intra- and inter-modular connectivity respectively. This allows the brain regions to be categorized into one of seven possible categories (see Methods), viz., R1: ultra-peripheral, R2: peripheral, R3: satellite connector, R4: kinless, R5: provincial hub, R6: connector hub, and R7: global hub. Note that there are no regions in the Macaque brain belonging to the categories R4 and R7. (b) The distribution of the regions of the entire Macaque brain across the different categories R1-R7 is similar to the corresponding distributions observed in several anatomical subdivisions, viz., *Tha*: Thalamus, *FL#2*: Frontal Lobe, *P1#6*: Parietal Lobe, *CgG#2*: Cingulate Gyrus, *Insula*, *TL#2*: Temporal Lobe, *OC#2*: Occipital Lobe, *Amyg*: Amygdala and *STR*: Striatum. (c) The connectivity pattern between regions belonging to the different categories R1-R7 indicated by the z-scores for abundance of links between each pair of categories (the first symbol in R_i - R_j refers to the category of the source region and the second to that of the target), measured with respect to degree- and modularity-preserved randomized ensemble of networks (see Methods). Large positive (or negative) z-scores, i.e., $z > 1$ (or $z < -1$), indicated by the dotted lines, imply that the corresponding connection types occur significantly more (or less) often than expected from random networks that have degree sequence and community structure identical to the empirical network. (d) Sagittal projection of the network of brain regions [see Fig. 1 (b)] showing that connections between provincial hubs (highlighted nodes) are localized within each module. (e) Temporal evolution of spreading processes, quantified in terms of distributions of first passage times (τ) of random walkers starting from one node to reach another, contrasted between the empirical brain network (solid line, τ_{emp}) and randomized ensembles of networks, generated by preserving either the degrees alone (red, τ_D), or both the degree and the modular membership of each node (green, τ_{DM}). (f) The distribution of τ differs significantly, depending on whether the target and source nodes belong to the same module (blue, τ^{intra}) or different modules (red, τ^{inter}). As in (e), spreading occurs significantly more rapidly in the empirical network (solid lines) compared to the networks belonging to the randomized ensemble (obtained by preserving degree and modular membership). In both (e) and (f), the dotted lines and the shaded regions around them represent the mean and standard deviation of $P(\tau)$ calculated over the randomized ensembles. To see how the different categories R1-R7 of brain regions allow spreading to occur faster in the empirical brain network than in equivalent randomized networks, we focus on the cases where the source nodes are either satellite connectors R3 (g) or provincial hubs R5 (h). The z-score indicates that there is a statistically significant shift in the empirical distribution towards lower values of τ in both cases. However, while for R3 the increase in the rate of spreading is similar, irrespective of whether the target is in the same module or in a different one, we observe that for R5, there is a relatively larger shift at lower values for τ^{intra} as compared to τ^{inter} . This is consistent with the connectivity pattern of provincial hubs with the other categories of nodes [shown in (c)] which particularly favors intra-modular communication.

We observe that every module comprises sizable number of both cortical and sub-cortical regions. With the exception of #3, the modules have their sub-cortical components located almost exclusively in the *Thalamus*. We note that each of these modules are associated with different sensory modalities (discussed in detail later), consistent with one of the primary functions of the *Thalamus*, namely, relaying information from the sensory organs to cortical areas for further processing. As the *Thalamus* is also involved in sleep-wake regulation coordinated via extensive reciprocal connections with the cortex [45–47], it is reasonable to expect that each of the network modules will have thalamic components along with cortical ones, with dense intra-modular connectivity representing thalamo-cortico-thalamic circuits [48, 49]. However, none of the sub-cortical components of module #3 (displayed in green in Fig. 1) belong to the *Thalamus* and instead constitutes almost the entirety of the *Basal Ganglia*.

The locations of the cortical components of the different modules across the principal lobes of the cortex, viz., *frontal*, *temporal*, *parietal* and *occipital*, are indicated in Fig. 1 (d). We observe that there is no simple correspondence between the modules, which are topological partitions of the connectome, and the gross anatomical subdivisions of the cortex. While the regions comprising the frontal and temporal lobes are split between several modules, those in the parietal and occipital are dominated by single modules (modules #2 and #5, respectively), indicating the relative homogeneity of the latter lobes in the mesoscopic organization of the network. This assumes importance in light of a possible connection between the modular divisions and functional specialization in the brain - a point that we discuss below.

As mentioned in the Introduction, the term *module* has been primarily used in the neuroscience literature to refer to a functionally integrated set of areas [50–52] that allows for “information encapsulation” [19], whereas we employ the term in the sense of a specific meso-level structural feature in the connectome [7–15]. In analogy with other biological networks where a structure-function correlation has been established for modules [40, 53], we now ask whether the network modules that appear as separate structural units of the brain can be considered as distinct functional units as well. Using information about the known functions of different cortical and sub-cortical areas obtained from decades of experimental studies, we have created a mapping between the regions belonging to each module and the specific functionalities attributed to them (see SI). A perusal of this information reveals that the different regions belonging to a module complement each other in carrying out various cognitive functions. For example, several cortical areas in module #5, viz., 45a and 8Ac of the pre-frontal cortex, and V1 and V2 of the occipital lobe, are related through their involvement in vision, even though they may be part of distinct lobes and have disparate functions (controlling saccadic eye movements in the case of 45a and 8Ac, and processing of visual information in the case of V1 and

V2). This suggests a general scheme of organization in which the regions associated with each of the principal sensory modalities are localized in specific modules, viz., visual in module #5, auditory in module #4, somatosensory (along with the principal motor area M1) in module #2 and olfactory (as well as, gustatory) in module #1. We show below that the known behavior of the regions comprising each of the modules is consistent with the broad functions attributed to that module.

First, we observe that module #5 (displayed in purple in Fig. 1) consists of the primary visual area in the occipital lobe and association areas in the parietal (e.g., LIP, VIP etc.) and temporal lobe (e.g., CIT, PIT, etc.). In addition, its thalamic component includes *lateral geniculate nucleus* (LGN), which relays visual information to the cortex from the retina. We note that these regions are all involved in various aspects of visual cognition, which is consistent with the sensory modality associated with this module, viz., vision. Second, module #4 (displayed in yellow in Fig. 1), consistent with its attributed sensory modality, is seen to comprise the auditory cortex lying in the superior temporal gyrus of the temporal lobe (as well as, the corresponding association areas), and the medial geniculate nucleus in the thalamus, which is the relay for all auditory information destined for the cortex from the brainstem [54]. Third, module #2 (displayed in red in Fig. 1), contains the primary and secondary somatosensory areas (S1, S2) in the parietal lobe, while its thalamic component contains all the regions which together comprise the ventral posterior nucleus that relays somatosensory information to the cortex. Apart from its sensory function, as noted earlier it also consists of primary and supplementary motor areas which are associated with planning, control and execution of voluntary movements [55]. Finally, we note that module #1 (displayed in blue in Fig. 1), has the *olfactory complex* and the *gustatory cortex*, both located in the frontal lobe, as well as, a few other regions (e.g., the olfactory field of the entorhinal cortex, EO, in the temporal lobe) involved in the sensory processing of smell. However, the module is dominated by association areas located in the prefrontal cortex which are involved in high-level multi-modal sensory integration and decision-making [56–60].

In contrast to the other modules, #3 neither contains motor areas nor does it include any primary or secondary sensory areas. This is possibly related to our earlier observation that this module has a distinct structural arrangement, in that its sub-cortical components do not have any contribution from the thalamus, but instead comprise regions belonging to the basal ganglia. In particular, the module contains the entire *amygdala* which is known to regulate emotional responses and fear-conditioning in mammals [61–64]. This gains significance in light of the fact that both the *Hippocampus* and the *Parahippocampus*, which are primarily involved in the formation of memory, feature prominently among this module’s cortical components. It resonates with the known relation between emotional state and formation

of memories in individuals that have been established by several studies [65–68].

As the brain is characterized by structures occurring at several scales [69], it is pertinent to ask whether further levels of organization can be identified in the connectivity pattern within each of the modules described above. Indeed, when we consider module#5, the most robust under different realizations of network partitioning (see Methods and SI), and subject it to further modular decomposition, we observe that it comprises three communities which we refer to as sub-modules. The largest of these contains the visual cortex and almost the entirety of the sub-cortical components, while the other two (which are comparable to each other in terms of the number of constituent regions) are dominated by regions belonging to the superior temporal sulcus and the intraparietal sulcus, respectively (see SI). Intriguingly, we note that the latter two communities appear to correspond to regions identified with different visual processing pathways, viz., the dorsal and ventral streams [70, 71].

B. Distribution profile of nodes in terms of their intra- and inter-modular connectivity is conserved across cortical and sub-cortical subdivisions

Having described the overall organizational structure of the network at the mesoscopic level, we now focus on understanding the role played by the individual brain regions in connecting other regions within their own module, as well as, across modules. The importance of each region is quantified in this framework by measuring the within-module degree z -score and the inter-modular participation coefficient P (see Methods for details). As seen in Fig. 2 (a), the z -score allows regions to be distinguished between *hubs*, i.e., those having significantly higher number of connections to other regions in their module, and *non-hubs*, while P further classifies the hubs into *provincial* (R5), *connector* (R6) and *global* (R7) categories and the non-hubs into *ultra-peripheral* (R1), *peripheral* (R2), *satellite connector* (R3) and *kinless* (R4) classes. We note that regions in each module have a similar distribution across R1-R3 and R5-R6 (with the sole exception of module #4 which has no region playing the role of a provincial hub, see SI). Uniformity of this nature can also be observed in Fig. 2 (b) where we compare the distributions of constituent regions across the different categories for the entire brain with that of the various subdivisions of the cortex, such as the Frontal (FL#2), Parietal (P1#6), Temporal (TL#2) and Occipital (OC#2) lobes, the Insula and the Cingulate Gyrus (CgG#2), as well as, the Amygdala (Amyg) which belongs to the basal ganglia. However, the Striatum which is also in the basal ganglia, and the Thalamus (Tha) have the distinctive characteristic of being essentially devoid of regions that act as hubs, indicating a relative lack of heterogeneity in the number of connections that their constituent regions have with others in their modules.

We have also analyzed the relative frequency with which regions belonging to the different categories connect to each other in the Macaque brain, compared to the corresponding connectivity pattern observed in surrogate networks obtained by degree- and modularity-preserving randomization (see Methods) [41]. The profile of connection preferences between the various categories shown in Fig. 2 (c), with under-representation of connections between R1-R1, R5-R6 and R6-R6 which has been related to the occurrence of multi-star structures, resembles other networks involved in information propagation [41]. As can also be seen from the figure, non-hubs prefer in general to connect to hubs and vice versa. This is indicative of degree disassortativity, i.e., connections between nodes having dissimilar characteristics (in this case, the number of connections) are favored. However, on investigating the connectivity between pairs of these categories, we notice that source regions belonging to peripheral (R2) and provincial hub (R5) categories show a distinct bias in their connections in terms of the participation coefficient of the target regions. Specifically R2 regions prefer to connect to connectors, both hubs (R6) and non-hubs (R3), while avoiding regions that are localized in their modules (R1, R2 and R5). The trend is reversed for R5 regions. In particular, they show a slight preference for connecting to each other, which is in contrast to the other categories which exhibit a marked tendency to avoid others of their own kind.

This homophily between provincial hubs could arise from two different patterns of connectivity between them, viz., one in which connections between the R5 regions are confined within the same module and another in which the corresponding regions across different modules are connected. Fig. 2 (d) shows that the empirical evidence supports the former arrangement where, within each module, provincial hubs connect to each other preferentially. We note that the three R5 regions indicated in module #5 occur, respectively, in the three different sub-modules that were identified in the previous subsection. This intra-modular connectivity within provincial hubs, taken together with the observation that they preferentially connect to peripheral regions while avoiding connectors, suggest that they help co-ordinate activity locally within each module while limiting the spread of information over the network.

C. Information spreading within the brain is enhanced by the specific pattern of intra- and inter-modular connections

The roles played by regions belonging to different categories in facilitating the transmission of information within and between modules can be investigated by considering a process of diffusive propagation across the network (see Methods). The distribution of first passage times τ , i.e., the time elapsed between initiating a random walk from any source node and the earliest arrival

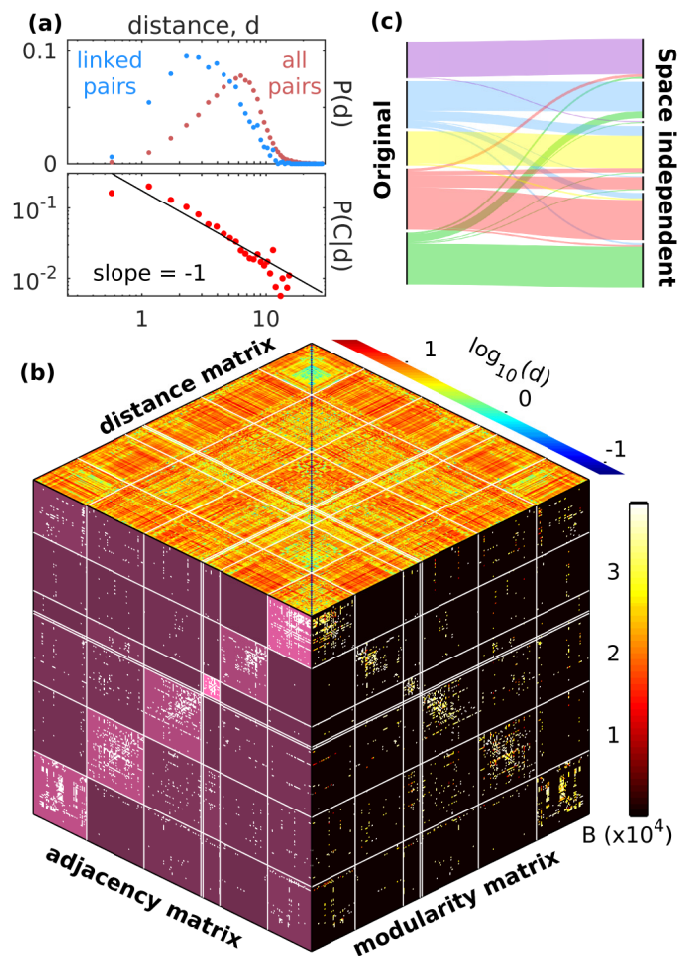


FIG. 3. **Physical distance between brain regions is seen to constrain their connectivity, but the modular organization of the network is independent of their three-dimensional spatial arrangement.** (a, top) Probability distribution of the physical distances d between all pairs of nodes (red) contrasted with that of connected pairs (blue). (a, bottom) The variation with physical distance d of the connection probability $P(C|d)$ between a pair of nodes separated by that distance (red). The empirical data is best fit by the relation $P \sim 1/d$ (represented by the solid line). (b) Joint representation of the space-independent modular organization of the network of brain regions showing the matrices indicating adjacency $\{A_{ij}\}$ (left surface), modularity $\{B_{ij}\}$ (normalized by total number of links L , right surface) and physical distance $\{d_{ij}\}$ (top surface) between the different regions. Note that for matrix \mathbf{A} the background intensity of each block is proportional to the density of connections within that block, and for matrix \mathbf{B} only the values corresponding to linked pairs of nodes are shown. The nodes are grouped into partitions corresponding to the space-independent modules of the network with the boundaries indicated by solid lines. The relatively large positive values clustered along the diagonal blocks of \mathbf{B} indicate the occurrence of significantly higher density of connections within each module, compared to that expected from the degrees of, and the distance between, every pair of nodes. This characteristic signature of modularity is also visible in the adjacency matrix \mathbf{A} representing the connection topology, suggesting that the mesoscopic structure of the brain network is a consequence of factors beyond the constraints associated with physical distance. Indeed, this is also true for the spatial clustering of nodes in each network module seen in Fig. 1 (a-c), as is apparent from the distance matrix showing that the modules comprise many nodes that are spatially proximal even after discounting the effect of distance in identifying the modules. (c) Visual representation of the correspondence between the network modules determined using exclusively information about the connection topology (“Original”) and those obtained from *space-independent* partitioning of the network into communities. on the right). This alluvial diagram has been created using the online visualization tool RAW [44].

to any given target node, is shown in Fig. 2 (e). While, in general, presence of modules in networks leads to slower global diffusion [22], surprisingly we observe that the distribution for the empirical network is markedly shifted towards lower values of τ compared to randomized networks with an identical degree sequence that

may or may not have modular organization. This indicates that, as opposed to information encapsulation, the specific pattern of intra- and inter-modular connections between brain regions belonging to different categories actually promotes faster communication across the network. Moreover, as seen from Fig. 2 (f), the enhancement

of the rate of diffusion in the connectome (in comparison to the randomized surrogates) can be seen both for transmission within a module, as well as, between different modules.

We also investigate how nodes having distinct intra- and inter-modular connectivity roles contribute to enhancing communication in the network. This is achieved in each case by having the source node belong to the respective category and comparing the corresponding distribution of τ with that obtained from randomized surrogates (quantified using z -score, see Methods). Fig. 2 (g) shows that starting from a satellite connector R3, diffusion to other nodes belonging both within its module or to other modules is significantly faster compared to randomized networks with identical modular organization and degree distribution. In contrast, as seen from Fig. 2 (h), when starting from a provincial hub R5, the increase in the rate of diffusion within a module, compared to that in the surrogate networks, is even higher than the increase in the rate of diffusion across modules. This resonates with the observation of homophily between provincial hubs in a module reported earlier (Fig. 2 (d)). When the source node belongs to any of the other categories, the difference between the intra- and inter-modular diffusion time-scales is seen to lie between the range seen for these two cases (see SI). This suggests that the modular character of the mesoscopic organization of the connectome is further shaped by the distribution of roles played by the different nodes in allowing information to spread within a module, as well as, across different modules.

D. Spatial layout constrains the connectivity but does not determine the modular organization of brain regions

So far we have investigated the modular structure of the network of brain regions exclusively in terms of the connection topology. However, the brain is also a physical system that is embedded in three-dimensional space associated with a distance metric which restricts the possible connections between its constituent regions. Such constraints arise from resource costs related to the spatial volume and transmission time associated with the connections, and the rapid energy consumption during synaptic transmission [72–78]. Thus, given that the pattern of connections between the regions is a function of the physical distance between them, we can ask to what extent are the modules a consequence of the brain being a spatially embedded network [79]. To investigate the role of spatial constraints on the structure of the brain network, we supplement the network topological information with that of the physical locations and volumes of each of the regions (shown in Fig. 1, a-c; for details see Methods). By comparing the distributions of the physical distances d between all possible pairs of regions (connected or not) with that of only the connected pairs [top

panel of Fig. 3 (a)], we can obtain the dependence of the connection probability between two regions on the distance d between them. As seen from the bottom panel of Fig. 3 (a), this probability decays linearly with the reciprocal of the distance, i.e., $P(C|d) \sim 1/d$, explicitly demonstrating the constraint imposed by the spatial layout of the brain regions on their connectivity.

To see if the restriction on long-range connections implied by the above constraint is responsible for the mesoscopic organization of the network we have reported here, we investigate whether the network can be partitioned into modules even after taking into account the distance dependence of the connection probability in the null model (see Methods for details). Thus, if the modules are exclusively a product of the distance constraint, the deviation of the empirically obtained connection probabilities from those of the null model will be minimal, yielding a single partition comprising the entire network (see SI for results on different surrogate networks). In contrast to the above scenario, we find that applying the method on the brain network yields an optimal partitioning comprising seven space-independent modules indicated by the diagonal blocks demarcated by white lines in the adjacency matrix shown in Fig. 3 (b) [left surface]. The probability of connections within these modules deviate strongly from the values expected from the null model as shown by the modularity matrix [Fig. 3 (b), right surface]. The distance matrix [Fig. 3 (b), top surface] also appears to suggest that regions belonging to the same module are, in general, physically closer to each other than those belonging to different modules. However, this physical proximity cannot provide a causal explanation for the modular structure as, even after filtering for spatial effects, the resulting space-independent modules are substantially similar to those reported in the previous subsections [see Fig. 3 (c)]. The similarity between the results of these two different modular partitionings is quantitatively indicated by the corresponding normalized mutual information $I_{\text{norm}} (= 0.6)$ [see Methods]. Thus, the spatial layout of the brain regions cannot by themselves explain the mesoscopic organization of the network, and the existence of the structural modules is a fundamental attribute of the brain.

IV. DISCUSSION

Despite differences in the details of their organization, the modules that we have identified in the Macaque connectome have common structural features. Most notably, each of them have cortical and thalamic components with the sole exception of module #3, suggesting a distinct functionality of this module. The sizable thalamic contribution to modules #2, #4 and #5 can be understood in terms of the roles that their cortical components play in processing specific sensory modalities. In particular, the information from the corresponding sensory organs arrive at the cortical regions belonging to these modules

via relay centers located in the thalamic component of the respective modules. This, however, cannot explain the sizable contribution from thalamic regions to module #1, as the sensory modalities it is associated with, namely, olfaction and gustation, do not involve any thalamic relay. As one of the primary functions of this module is the integration of information processed in different cortical regions (as mentioned earlier), it suggests that regions in the thalamic component of this module serve as relay centers coordinating inter-cortical communication [45].

The module with which a particular brain region is associated may also alert us to possible functions of this region that have not yet been identified. As an example we consider multi-modal association areas, which integrate and process inputs from different sensory modalities (such as the regions *LIP*, *MIP* and *area 46*). Using information about their modular membership, we can identify which modality or function each of these regions are most strongly associated with. This is illustrated by considering the *LIP*, *VIP*, *AIP* and *MIP* areas of the *Intraparietal Sulcus*. Although they are all multi-modal association areas, *LIP* and *VIP* are part of module #5, whereas areas *AIP* and *MIP* are part of module #2. It is known that *LIP* and *VIP* are involved in visual attention and saccadic eye movements [80–82], which are predominantly visual processing tasks (consistent with the broad function of module #5). In contrast, *AIP* and *MIP* coordinate the visual control of reaching and pointing [83–85], which, although guided by visual information, is primarily a motor function (consonant with the broad function of module #2). Thus, the specific functionalities of these association areas seem to tie in with the modules that they belong to.

We note that the modular nature of the brain has been long recognized, both in terms of function and, more recently, in the topological organization of its structural connections [15]. Considerable attention has been focused on the question of structure-function convergence in the context of brain modules [20]. The hypothesis of “information encapsulation”, whereby it is assumed that the information processing related to specific functions are relatively unaffected by those corresponding to other functions, has been suggested as an explanation of how functional modules can arise from the structural organization of the connectome into several communities [86]. Although this may appear intuitive because spreading processes are generally fast within a module and slow down during their passage to a different module [22], we find on the contrary that the specific modular organization of the Macaque connectome allows signals to spread very fast. In fact, the communication of information across the empirical network appears to be even faster than that seen in equivalent networks whose connections are distributed homogeneously. This is surprising as homogeneous networks tend to exhibit the fastest speed of propagation globally, which usually tends to reduce once mesoscopic structural features such as modularity are in-

roduced [22]. We connect this counter-intuitive result to the detailed meso-level attributes of the topological organization, specifically the roles played by different brain regions in terms of their intra- and inter-modular connections. By analyzing these connections we reveal distinctive features of the connectome, namely, the tendency of provincial hubs within a module to connect to each other, and the preference shown by connector hubs to link to peripheral nodes across different modules.

While the potential of rapid communication between different regions, made possible by the underlying modular architecture of the network, suggests a plausible explanation for the evolution of the observed mesoscopic organization of the macaque brain, it could also plausibly be a consequence of optimizing for wiring lengths. However, we have explicitly shown that the constraint imposed by the physical distance between the brain regions is insufficient to explain the modular partitions observed by us. Indeed, although the five modules of the connectome that we have identified comprise brain regions that are, for the most part, spatially proximal, module #4 is a prominent exception. It spans two widely separated locations in the brain, one comprising the primary and secondary auditory areas which are in the temporal lobe and the other consisting of association areas located in the prefrontal lobe. While it is well-established that the temporal lobe regions belonging to this module contribute to its associated sensory modality, viz., auditory processing, it is not entirely clear what role the prefrontal regions of this module plays in this context. We note, however, that there are intriguing parallels between these areas and those occupying corresponding locations in the human brain. Specifically, the prefrontal and temporal parts of module #4 that are known to have a role in social cognition in primates [87, 88] correspond to the Broca’s and Wernicke’s areas in the human brain, respectively. As is well known, the former is responsible for speech production in humans, while the latter is critical for language comprehension [55]. Although there is no direct counterpart of language in Macaques, non-human primates are known to be capable of communicating through signals such as facial expressions and vocalizations [89]. This correspondence therefore warrants consideration of whether some of the areas in module #4 of the Macaque brain developed from a common evolutionary precursor of the apparatus responsible for facilitating language in humans. Indeed, this view is supported by recent research [90–92] that have used language-like behavior in non-human primates as models for understanding how speech and language might have evolved in humans [93].

ACKNOWLEDGMENTS

We would like to thank Raghavendhra Singh, Sridharan Devarajan and Dipanjan Ray for helpful discussions. SNM has been supported by the IMSc Complex Systems Project (12th Plan), and the Center of Excellence

in Complex Systems and Data Science, both funded by the Department of Atomic Energy, Government of India. The simulations and computations required for this work

were supported by High Performance Computing facility (Nandadevi and Satpura) of The Institute of Mathematical Sciences, which is partially funded by DST.

-
- [1] K. Zilles and K. Amunts, *Nat Rev Neurosci* **11**, 139 (2010).
- [2] A. Goulas, R. F. Betzel, and C. C. Hilgetag, *Sci Adv* **5**, eaav9694 (2019).
- [3] L. W. Swanson and M. Bota, *Proc Natl Acad Sci USA* **107**, 20610 (2010).
- [4] P. T. Fox and K. J. Friston, *Neuroimage* **61**, 407 (2012).
- [5] K. Friston, *Annu Rev Neurosci* **25**, 221 (2002).
- [6] G. Deco, V. K. Jirsa, P. A. Robinson, M. Breakspear, and K. Friston, *PLoS Comput Biol* **4**, e1000092 (2008).
- [7] J. W. Scannell, G. A. P. C. Burns, C. C. Hilgetag, M. A. O’Neil, and M. P. Young, *Cereb Cortex* **9**, 277 (1999).
- [8] C. C. Hilgetag, G. A. P. C. Burns, M. A. O’Neill, J. W. Scannell, and M. P. Young, *Philos Trans R Soc London, Ser B* **355**, 91 (2000).
- [9] D. S. Bassett, D. L. Greenfield, A. Meyer-Lindenberg, D. R. Weinberger, S. W. Moore, and E. T. Bullmore, *PLoS Comput Biol* **6**, e1000748 (2010).
- [10] R. K. Pan, N. Chatterjee, and S. Sinha, *PLoS One* **5**, e9240 (2010).
- [11] Q. Wang, O. Sporns, and A. Burkhalter, *J Neurosci* **32**, 4386 (2012).
- [12] L. Harriger, M. P. Van Den Heuvel, and O. Sporns, *PloS One* **7**, e46497 (2012).
- [13] M. Shanahan, V. P. Bingman, T. Shimizu, M. Wild, and O. Güntürkün, *Front Comput Neurosci* **7**, 89 (2013).
- [14] C.-T. Shih, O. Sporns, S.-L. Yuan, T.-S. Su, Y.-J. Lin, C.-C. Chuang, T.-Y. Wang, C.-C. Lo, R. J. Greenspan, and A.-S. Chiang, *Curr Biol* **25**, 1249 (2015).
- [15] O. Sporns and R. F. Betzel, *Annu Rev Psychol* **67**, 613 (2016).
- [16] Y. Chen, Z.-K. Zhang, Y. He, and C. Zhou, *Cereb Cortex* (2020), 10.1093/cercor/bhaa060.
- [17] D. Meunier, R. Lambiotte, and E. T. Bullmore, *Front Neurosci* **4**, 200 (2010).
- [18] R. K. Pan and S. Sinha, *Phys Rev E* **76**, 045103 (2007).
- [19] J. A. Fodor, *The Modularity of Mind* (MIT Press, Cambridge MA, 1983).
- [20] H.-J. Park and K. Friston, *Science* **342**, 1238411 (2013).
- [21] L. W. Swanson and J. W. Lichtman, *Annu Rev Neurosci* **39**, 197 (2016).
- [22] R. K. Pan and S. Sinha, *EPL* **85**, 68006 (2009).
- [23] D. Mumford, *Biol Cybern* **65**, 135 (1991).
- [24] C. G. Antonopoulos, S. Srivastava, S. E. d. S. Pinto, and M. S. Baptista, *PLoS Comput Biol* **11**, e1004372 (2015).
- [25] Y. Yamaguti and I. Tsuda, *Neural Netw* **62**, 3 (2015).
- [26] R. F. Betzel, J. D. Medaglia, L. Papadopoulos, G. L. Baum, R. Gur, R. Gur, D. Roalf, T. D. Satterthwaite, and D. S. Bassett, *Network Neuroscience* **1**, 42 (2017).
- [27] J. Stiso and D. S. Bassett, *Trends Cogn Sci* **22**, 1127 (2018).
- [28] D. S. Modha and R. Singh, *Proc Natl Acad Sci USA* **107**, 13485 (2010).
- [29] K. E. Stephan, K. Zilles, and R. Ktter, *Philos Trans R Soc London, Ser B* **355**, 37 (2000).
- [30] K. E. Stephan, L. Kamper, A. Bozkurt, G. A. P. C. Burns, M. P. Young, and R. Ktter, *Philos Trans R Soc London, Ser B* **356**, 1159 (2001).
- [31] R. Kötter, *Neuroinformatics* **2**, 127 (2004).
- [32] <https://scalablebrainatlas.incf.org/macaque/PHT00>.
- [33] G. Paxinos, X. F. Huang, and A. W. Toga, *The Rhesus Monkey Brain in Stereotaxic Coordinates* (Academic Press, San Diego, CA, 2000).
- [34] M. E. J. Newman, *Eur Phys J B* **38**, 321 (2004).
- [35] M. E. J. Newman and M. Girvan, *Phys Rev E* **69**, 026113 (2004).
- [36] M. E. J. Newman, *Proc Natl Acad Sci USA* **103**, 8577 (2006).
- [37] B. H. Good, Y. A. De Montjoye, and A. Clauset, *Phys Rev E* **81**, 046106 (2010).
- [38] <http://tuvalu.santafe.edu/~aaronc/modularity/>.
- [39] M. Rosvall and C. T. Bergstrom, *Proc Natl Acad Sci USA* **105**, 1118 (2008).
- [40] R. Guimerà and L. A. N. Amaral, *Nature (London)* **433**, 895 (2005).
- [41] R. Guimera, M. Sales-Pardo, and L. A. N. Amaral, *Nat Phys* **3**, 63 (2007).
- [42] P. Expert, T. S. Evans, V. D. Blondel, and R. Lambiotte, *Proc Natl Acad Sci USA* **108**, 7663 (2011).
- [43] D. J. C. MacKay, *Information Theory, Inference and Learning Algorithms* (Cambridge University Press, Cambridge, UK, 2003).
- [44] M. Mauri, T. Elli, G. Caviglia, G. Uboldi, and M. Azzi, in *Proceedings of the 12th Biannual Conference on Italian SIGCHI Chapter*, CHIItaly ’17 (ACM, New York, NY, USA, 2017) pp. 28:1–28:5.
- [45] J. N. MacLean, B. O. Watson, G. B. Aaron, and R. Yuste, *Neuron* **48**, 811 (2005).
- [46] L. J. Van Hemmen and T. J. Sejnowski, *23 Problems in Systems Neuroscience*, Computational Neuroscience Series (Oxford University Press, USA, 2006).
- [47] M. Steriade, D. A. McCormick, and T. J. Sejnowski, *Science* **262**, 679 (1993).
- [48] R. W. Guillery, *J Anat* **187**, 583 (1995).
- [49] S. M. Sherman and R. W. Guillery, *J Neurophysiol* **76**, 1367 (1996).
- [50] C. M. J. Braun, M. Dumont, J. Duval, I. Hamel-Hébert, and L. Godbout, *J Psychiatry Neurosci* **28**, 432 (2003).
- [51] S. Sternberg, *Cogn Neuropsychol* **28**, 156 (2011).
- [52] M. S. Gazzaniga, in *Self and Consciousness* (Psychology Press, Abingdon, UK, 2014) pp. 96–110.
- [53] L. H. Hartwell, J. J. Hopfield, S. Leibler, and A. W. Murray, *Nature (London)* **402**, C47 (1999).
- [54] D. E. Purves, G. J. Augustine, D. E. Fitzpatrick, W. C. Hall, A.-S. E. LaMantia, J. O. McNamara, and L. E. White, *Neuroscience* (Sinauer Associates, Sunderland (MA), Sunderland, MA, 2001).
- [55] E. Kandel, J. Schwartz, and T. Jessell, *Principles of Neural Science, Fourth Edition*, Vol. 4 (McGraw-hill, New York, 2000).
- [56] M. E. Walton, T. E. J. Behrens, M. J. Buckley, P. H.

- Rudebeck, and M. F. S. Rushworth, *Neuron* **65**, 927 (2010).
- [57] L. K. Fellows, *Ann N Y Acad Sci* **1121**, 421 (2007).
- [58] M. E. Walton, J. T. Devlin, and M. F. S. Rushworth, *Nat Neurosci* **7**, 1259 (2004).
- [59] A. Izquierdo, R. K. Suda, and E. A. Murray, *J Neurosci* **24**, 7540 (2004).
- [60] E. T. Rolls, *Cereb Cortex* **10**, 284 (2000).
- [61] L. Weiskrantz, *J. Comp. Physiol. Psychol.* **49**, 381 (1956).
- [62] M. Davis, *Annu Rev Neurosci* **15**, 353 (1992).
- [63] S. Killcross, T. W. Robbins, and B. J. Everitt, *Nature (London)* **388**, 377 (1997).
- [64] S. Maren, *Trends Neurosci* **22**, 561 (1999).
- [65] E. A. Kensinger and S. Corkin, *Mem Cogn* **31**, 1169 (2003).
- [66] M. P. Richardson, B. A. Strange, and R. J. Dolan, *Nat Neurosci* **7**, 278 (2004).
- [67] A. K. Anderson, P. E. Wais, and J. D. E. Gabrieli, *Proc Natl Acad Sci USA* **103**, 1599 (2006).
- [68] A. Tambini, U. Rimmele, E. A. Phelps, and L. Davachi, *Nat Neurosci* **20**, 271 (2017).
- [69] P. S. Churchland and T. J. Sejnowski, *Science* **242**, 741 (1988).
- [70] M. A. Goodale and A. D. Milner, *Trends Neurosci* **15**, 20 (1992).
- [71] M. A. Goodale and A. D. Milner, *Cortex* **98**, 283 (2018).
- [72] E. Bullmore and O. Sporns, *Nat Rev Neurosci* **13**, 336 (2012).
- [73] B. B. Averbeck and M. Seo, *PLoS Comput Biol* **4**, e1000050 (2008).
- [74] S. Herculano-Houzel, B. Mota, P. Wong, and J. H. Kaas, *Proc Natl Acad Sci USA* **107**, 19008 (2010).
- [75] D. B. Chklovskii, *Neural Comput* **16**, 2067 (2004).
- [76] M. Kaiser and C. C. Hilgetag, *Neurocomputing* **58**, 297 (2004).
- [77] G. Buzsáki, C. Geisler, D. A. Henze, and X.-J. Wang, *Trends Neurosci* **27**, 186 (2004).
- [78] J. E. Niven and S. B. Laughlin, *J Exp Biol* **211**, 1792 (2008).
- [79] M. Barthélemy, *Phys Rep* **499**, 1 (2011).
- [80] J. W. Gnadt and R. A. Andersen, *Exp Brain Res* **70**, 216 (1988).
- [81] J.-R. Duhamel, C. L. Colby, and M. E. Goldberg, *J Neurophysiol* **79**, 126 (1998).
- [82] B. Pesaran, J. S. Pezaris, M. Sahani, P. P. Mitra, and R. A. Andersen, *Nat Neurosci* **5**, 805 (2002).
- [83] H. Sakata, M. Taira, A. Murata, and S. Mine, *Cereb Cortex* **5**, 429 (1995).
- [84] E. N. Eskandar and J. A. Assad, *Nat Neurosci* **2**, 88 (1999).
- [85] C. Grefkes and G. R. Fink, *J Anat* **207**, 3 (2005).
- [86] M. Colombo, *Philos Sci* **80**, 356 (2013).
- [87] J. Sallet, R. B. Mars, M. P. Noonan, J. L. Andersson, J. X. O'Reilly, S. Jbabdi, P. L. Croxson, M. Jenkinson, K. L. Miller, and M. F. S. Rushworth, *Science* **334**, 697 (2011).
- [88] M. L. Platt, R. M. Seyfarth, and D. L. Cheney, *Phil Trans R Soc B* **371**, 20150096 (2016).
- [89] D. L. Cheney and R. M. Seyfarth, *Proc Natl Acad Sci USA* **115**, 1974 (2018).
- [90] B. Wilson, Y. Kikuchi, L. Sun, D. Hunter, F. Dick, K. Smith, A. Thiele, T. D. Griffiths, W. D. Marslen-Wilson, and C. I. Petkov, *Nat Commun* **6**, 8901 (2015).
- [91] C. T. Snowdon, *Science* **355**, 1120 (2017).
- [92] J. P. Rauschecker, *Curr Opin Behav Sci* **21**, 195 (2018).
- [93] O. Kolodny and S. Edelman, *Phil Trans R Soc B* **373**, 20170052 (2018).

SUPPLEMENTARY INFORMATION FOR

Mesoscopic architecture enhances communication across the Macaque connectome revealing structure-function correspondence in the brain

Anand Pathak^{1,2}, Shakti N. Menon¹ and Sitabhra Sinha^{1,2}

¹ The Institute of Mathematical Sciences, CIT Campus, Taramani, Chennai 600113, India

² Homi Bhabha National Institute, Anushaktinagar, Mumbai 400 094, India

1 The Structure of the Macaque Connectome

The data describing the Macaque connectome that we have used in our analysis are included in two files that are part of the Supplementary Information. The file `connectome_nodes.xls` is a spreadsheet comprising 11 columns which contain information about each of the 266 brain regions which correspond to the nodes of the network. The first 7 columns provide the identity of the region in terms of the serial number by which they are identified in our study, the abbreviation, the name, their position in the Macaque brain described in terms of the 3-dimensional coordinates as per the Paxinos atlas and the volume that they occupy. The eighth and ninth columns contain information arising from our analysis, viz., the module they belong to and their role in the mesoscopic organization (described in the main text), respectively. The last two columns contain, respectively, the references and the web resource from which we have gleaned information about their positions and volumes.

The file `connectome_links.dat` is an adjacency list containing information about the directed connections between the different nodes (brain regions) via anatomical tracts, with the first column indicating the source node and the second column the target node (both nodes being represented by their serial number as given in the file `connectome_nodes.xls`).

Fig. S1 shows some of the macroscopic properties of the network, viz., the cumulative distributions for the number of in-coming, out-going and total connections, and the correlation between the number of in-coming and out-going connections for each node. Fig. S1 (a) shows that the total degree distribution of the nodes [shown in the bottom panel] follows an exponential distribution, in agreement with the observed properties of the network investigated by Modha and Singh [1]. This suggests that the network that we have worked with, which has been processed extensively from the original network of 383 nodes (which contained many redundancies, as explained in the main text), shares the same macroscopic features as the original network. The top and middle panels show the in-degree and out-degree distributions. While both of these appear to also follow an exponential form, the former shows a deviation in the tail indicating that there exist regions that have more in-coming connections than is expected given the form of the distribution. In particular, the four nodes having the highest in-degrees [top panel] that show the largest deviation from the best-fit exponential distribution are all located in the pre-frontal cortex and are also seen to belong to the same module, viz., #1. This is in accordance with the known cognitive function of prefrontal cortex regions which is high-level multi-modal sensory integration.

In order to see whether regions which attract many in-coming connections also tend to have many out-going connections, we have looked at the correlation between in- and out-degrees in terms of a scatter plot [Fig. S1 (b)]. Here the nodes are colored according to the module to which they belong, while the relative volumes are represented by the size of the corresponding markers. We note that while most of the nodes are fit well by a linear relation between in-degree and out-degree, there does appear to be several nodes which have a disproportionately higher number of out-going connections than is expected from their in-degree, given the linear relation between the two. Specifically, there are 38 nodes whose out-degree deviate significantly from the value that is expected from the best-fit linear relation with their in-degree, i.e., they are larger than the upper bound given by the root mean square deviation (the upper lighter curve, see figure caption for details). Although the membership of these outliers span across all modules and functional

categories (in terms of the role they play in the mesoscopic organization of the connectome), we note that 32% of all connector hubs (R6) and 26% of all satellite connectors (R3) belong to these outliers. As nodes belonging to both of these categories are characterized by having their connections are distributed over several modules, it suggests a possible functional importance of the outlier nodes in coordinating information processing in the Macaque brain.

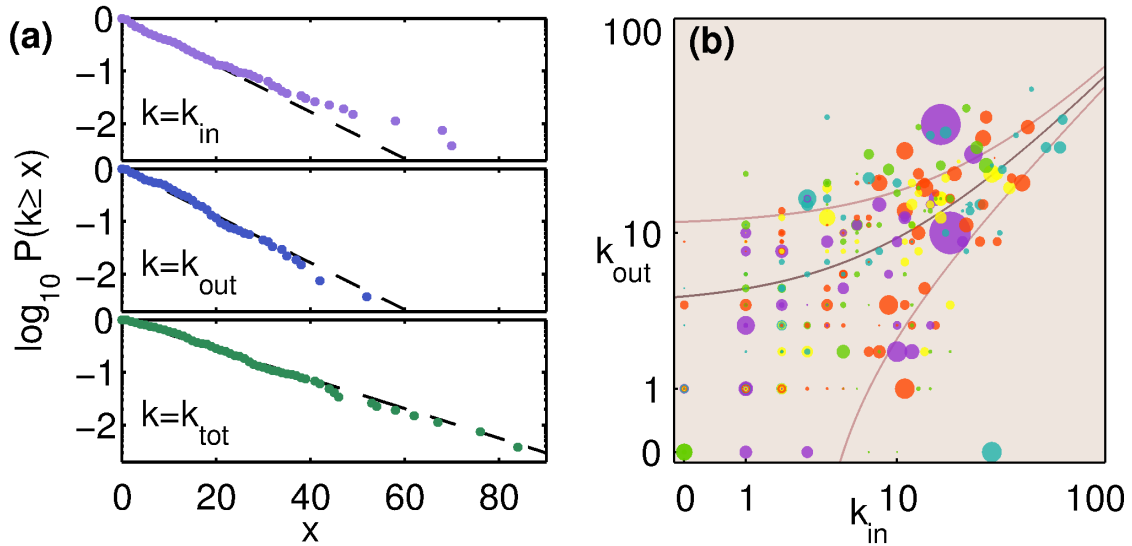


Figure S1: (a) The distributions of the (top) in-degree, (center) out-degree and (bottom) total degree of the Macaque connectome, indicating the best-fit exponential distribution (broken line) in each case. (b) Scatter plot indicating the correlation between in-degree and out-degree of the different nodes in the connectome. The relatively darker central curve represents the best-fit linear relation between k_{in} and k_{out} (the linear correlation coefficient is $r = 0.62$, with a p -value of 0) corresponding to a slope of 0.49. The two lighter curves on either side indicate the root mean square deviation of the empirical data from the best-fit linear relation. The color and sizes of the nodes are same as in Fig. 1 of the main text.

2 Modular Organization of the Connectome

2.1 Establishing the robustness of the modular decomposition

As described in the Methods section of the main text, we have ensured that the partitioning of the connectome is not sensitively dependent on the specific method used for the decomposition. Fig. S2 shows that the communities obtained using the Infomap method [2], which is based upon optimally compressing information about dynamic processes on the network, have a high degree of overlap with those obtained using a spectral method [3] that maximizes the modularity Q (for details, see Methods in main text). While the Infomap method generates a larger number of modules (specifically, 17), not only are many of these extremely small (in some cases comprising only a single node), but several of them are in fact further subdivisions of the relatively fewer modules (specifically, 5) obtained using the spectral method. The relatively high degree of correspondence between the partitions generated by using techniques that employ completely different principles suggests that the modular decomposition reported here is an intrinsic property of the network, and is not strongly affected by the partitioning method used.

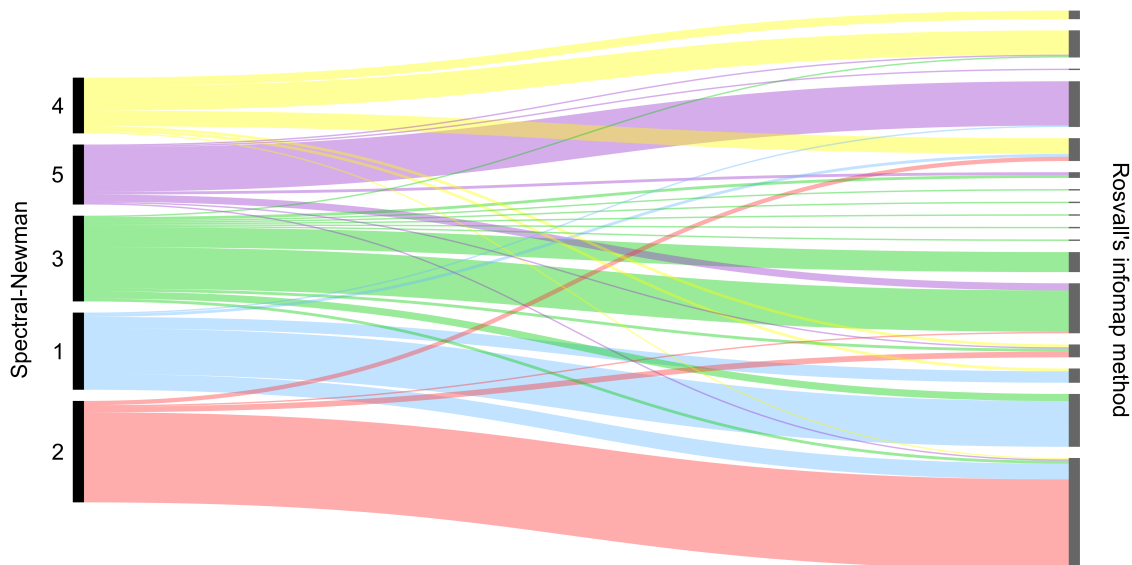


Figure S2: Visual representation of the comparison between the modular decomposition of the Macaque connectome obtained using spectral partitioning [left] with that obtained using the Infomap method [right]. The modules are represented as vertical bars, connected by bands which are colored according to the module obtained using the spectral method from which they originate [using the same color scheme as in Fig. 1 (d) of the main text]. This alluvial diagram has been created using the online visualization tool RAW [4].

To verify that the method used for maximizing Q does not alter our results significantly, we have performed 10^3 realizations of a stochastic simulated annealing algorithm for detecting communities [5]. As mentioned in the Methods (see main text), by comparing between these large number of optimal partitionings of the network, we can determine the extent to which the modular groupings among the different nodes is robust. Fig. S3 shows the Modularity Q values corresponding to these realizations, using a representation such that similar partitionings (corresponding to the circles) occur close to each other in the two-dimensional plane orthogonal to the axis representing Q . The two-dimensional coordinates of each circle in this plane is obtained by Curvilinear Component Analysis (CCA, see Ref. [6]) as described in Ref. [5].

As can be seen from Fig. S3, there are a large number of partitionings having high values of Q that occur close to each other in the plateau and where the partition obtained from the spectral method (diamond, having a Q -value of $Q_{spectral} = 0.485$) that has been for our analysis is also

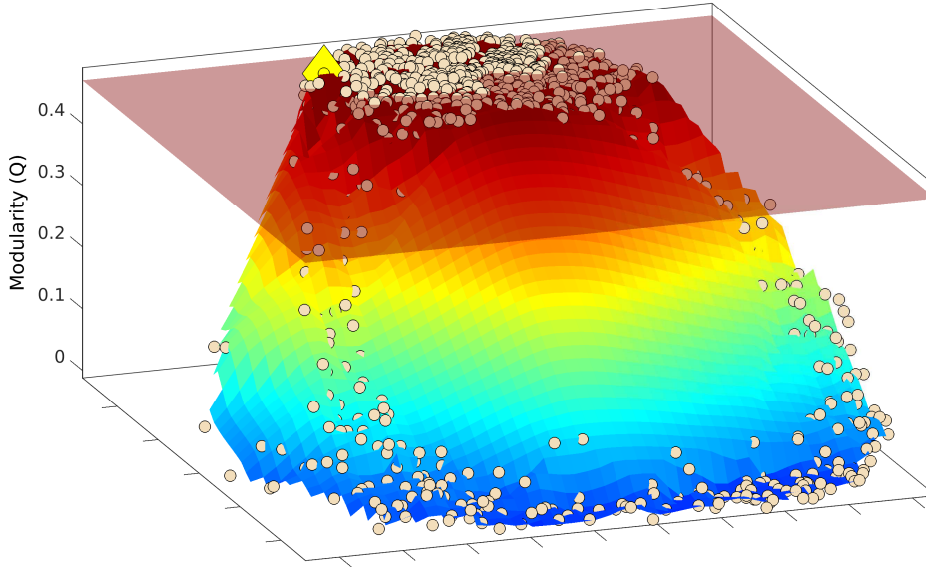


Figure S3: Modularity of the Macaque connectome, shown as a function reconstructed from 10^3 partitionings (circles) obtained through a simulated annealing method for determining communities [5]. The axes on the horizontal plane orthogonal to the vertical axis that corresponds to modularity Q represent embedding dimensions that are themselves complex functions of the partition space, such that the scale of these axes are irrelevant. The distance between the partitionings (whose positions on the horizontal plane are obtained by CCA) are indicative of the degree of dissimilarity between the corresponding modular partitions of the network. The partition obtained by the deterministic spectral method yielding a Q -value of $Q_{spectral} = 0.485$ (diamond), and which has been used for our analysis, is seen to occur in the high-modularity plateau comprising a large number of similar partitions, all having a high value of Q . The 291 partitionings that occur at the top of this surface, whose Q values differ by less than 3% from $Q_{spectral} = 0.485$ (specifically, the circles lying above the translucent plane corresponding to $Q = 0.47$ shown in the figure), have been used to determine the robustness of the modular identities of the different nodes in the connectome, as shown in Fig. S4 (left).

seen. This suggests that the modular decomposition of the nodes in these high Q partitionings are similar to that determined by the spectral method. Fig. S4 shows the brain regions whose modular identity is invariant across all the partitionings whose Q differs by less than 3% (i.e., $Q > 0.47$, left panel) and 7% (i.e., $Q > 0.45$, right panel) from $Q_{spectral}$. The conserved modular memberships of a large fraction ($\sim 70\%$) of the brain regions across all the different partitionings possessing high modularity (highlighted nodes in Fig. S4 [left]; see Table S1 for their identities) emphasizes that the modular mesoscopic organization we have described here does not depend sensitively on the method used to partition the network, underlining that it is an intrinsic property of the Macaque connectome.

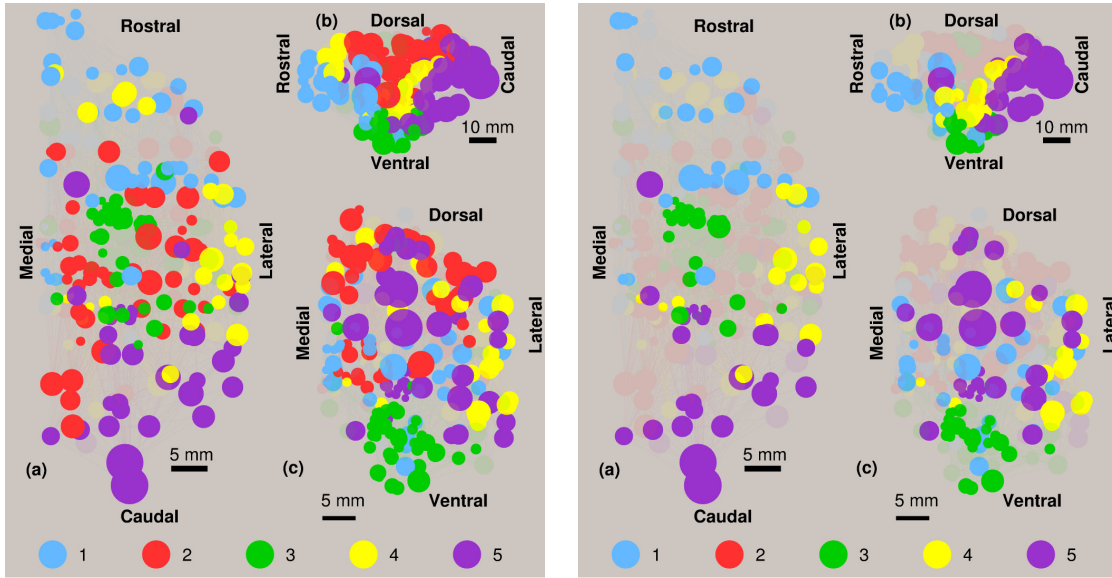


Figure S4: The network of brain regions shown in (a) horizontal, (b) sagittal and (c) coronal projections, indicating the regions (highlighted) whose modular memberships are invariant across the partitionings obtained by the spectral method (used in our analysis) as well as those obtained by simulated annealing, whose Q differs by less than (left) 3% and (right) 7% from $Q_{spectral} = 0.485$. As in Fig. 1 (a-c) in the main text, the modular membership of each node is represented by its color (see color key at the bottom of each panel), the spatial positions of the nodes are specified by the three-dimensional stereotaxic coordinates of the corresponding regions, and node sizes provide a representation of the relative volumes of the corresponding brain regions (the spatial scale being indicated by the horizontal bar shown next to each projection). (Left) Within the 291 partitionings that have $Q > 0.47$, around 70% of the 266 brain regions have the same modular membership as that seen in the spectral modular decomposition, underlining the robustness of their modular identities. (Right) For the 625 partitionings that have $Q > 0.45$, we see a much higher degree of variation in the modular identities of the regions across the partitionings as a result of including those with much lower values of Q . Specifically, modules #1, #3 and #5 are seen to have several nodes that are robust (i.e., consistently belong to the corresponding module) across the partitionings, while, for module #4, only some of the nodes belonging to the temporal lobe have this property. The nodes belonging to module #2, on the other hand, change from one partitioning to another.

Table S1: Brain regions highlighted in Fig. S4 (left) whose modular membership is conserved across all the 291 distinct partitionings with $Q > 0.47$, arranged according to the modules, and subsequently into the largest anatomical subdivision (viz., lobe / nuclei), to which they belong. For each region, the corresponding within-module degree z-score and the participation coefficient are displayed in the last two columns (see Methods for details).

Module #1			
Lobe/nuclei	region	zscore	pcoeff
FL	14r	1.154	0.344
	13L	0.481	0.148
	13M	0.443	0.102
	13a	2.837	0.471
	32	3.061	0.688
	10m	-0.230	0.000
	10v	-0.791	0.000
	10d	-0.866	0.000
	10o	0.443	0.000
	12o	2.613	0.619
	12m	0.593	0.263
	12r	0.107	0.069
	12l	2.239	0.659
	11l	0.368	0.108
	11m	1.042	0.447
	PrCO	0.032	0.559
6Vb	-0.305	0.457	
6Va	-0.267	0.438	
TL	TPag	-0.529	0.000
	TPg	-0.305	0.000
	TPdgv	-0.604	0.000
	TPdgd	-0.604	0.000
	Su#2	-0.754	0.000
	Sb	-0.754	0.000
cing	24b	0.780	0.549
Insula	Ial	-0.267	0.000
	Iam	0.630	0.373
	Iapm	0.705	0.515
	Iai	1.752	0.432
Thal	AM#1	-0.492	0.569
	Cim	-0.828	0.000
	Cif	-0.716	0.444
	Cdc	-0.754	0.560
	MDcd	-0.828	0.000
	MDpm	-0.754	0.000
	MDfi	-0.679	0.000
BG	SI#2	0.219	0.410
	Pu_r	0.219	0.429
OFC	OFC	-0.679	0.408
Module #2			
Lobe/nuclei	region	zscore	pcoeff
FL	F5	2.706	0.515
	4c	-0.575	0.180
	F4	0.807	0.355
	F7	3.512	0.551
	F2	2.418	0.360
	M2-FL	-0.862	0.480
	F6	1.267	0.512
	M1-FL	2.073	0.256

	MI-of	-0.402	0.272
PL	1#1	0.691	0.174
	2#1	0.634	0.121
	3b	0.346	0.322
	3a	0.173	0.227
	SII-f	-0.920	0.000
	PR#4	-0.690	0.000
	PFop	-0.805	0.000
	PGop	-0.690	0.000
	PFG#1	0.404	0.140
	PF#1	0.807	0.353
	AIP	-0.517	0.165
	MIP	0.749	0.307
	PEm	0.979	0.463
	5_Foot	-1.035	0.000
	PEc#1	1.152	0.228
	PGm	2.188	0.627
	PECg	1.267	0.399
OL	V6A	0.231	0.375
cing	24d	-0.114	0.290
	23c	2.188	0.563
	TSA	-0.057	0.355
Insula	Ri#1	-0.632	0.494
Thal	Pcn	0.289	0.650
	CM#2	0.231	0.226
	Csl	-0.287	0.640
	Ret	-0.287	0.338
	Pul.o	0.576	0.291
	X	-0.287	0.427
	VPS	-0.862	0.000
	VPM	-0.460	0.278
	VPLo	-0.517	0.000
	VPLc	-0.057	0.194
	VLm	-0.575	0.180
	VLps	-0.575	0.320
	VLo	0.058	0.308
	VLc	-0.114	0.198
VApC	-0.460	0.375	
BG	Pu_c	-0.460	0.375
Module #3			
Lobe/nuclei	region	zscore	pcoeff
TL	TFM	-0.309	0.000
	TFL	0.190	0.254
	35	2.044	0.469
	36c	1.117	0.111
	36r	2.329	0.177
	36p	-0.452	0.000
	EI	0.547	0.453
	ER#1	0.048	0.499
	28m	-0.594	0.180
	ECL	-0.309	0.408

	EC#2	0.689	0.487
	Pros.	-0.166	0.430
	PaS	-0.737	0.406
	TH	3.327	0.666
	PrS	-0.452	0.514
	CA1	0.333	0.159
	DG	-0.808	0.245
cing	29d	-0.951	0.560
BG	Bla	0.261	0.442
	Abpc	0.832	0.320
	Bi	0.903	0.412
	ABd	0.261	0.000
	Bvl	-0.024	0.000
	ABv	0.261	0.000
	MB	-0.024	0.290
	ABvm	0.547	0.204
	ABmg	0.832	0.420
	A	-0.095	0.111
	I#2	-0.879	0.278
	ME#1	-0.166	0.430
	CE#1	-0.095	0.360
	AHA	-0.594	0.180
	PAC2	-0.238	0.000
	COp	-0.808	0.000
	NLOT	-0.808	0.000
	COa	-0.523	0.397
	Ldi	1.117	0.216
	Ld#2	-0.166	0.219
Lv	0.974	0.229	
Lvl	0.618	0.137	
Module #4			
Lobe/nuclei	region	zscore	pcoeff
FL	M9	0.227	0.677
	D9	-0.257	0.602
	46v	2.437	0.741
	46d	0.848	0.477
	8B	2.299	0.629
TL	A1	0.641	0.340
	STPg	-0.326	0.418
	ProK	-0.326	0.231
	paAc	0.089	0.381
	L#1	0.019	0.320
	CL#4	-0.671	0.480
	AL#4	-0.464	0.426
	ST3	1.194	0.370
	ST2	0.641	0.445
	ST1	0.227	0.469
	Tpt	0.848	0.461
	TPOc	0.710	0.571
	TPOr	-0.257	0.492
	TAa	0.434	0.441

Thal	MG	-0.533	0.000
	SG	-0.188	0.519
	Li	0.019	0.615
Module #5			
Lobe/nuclei	region	zscore	pcoeff
FL	45A	0.385	0.562
	8Ac	-1.003	0.000
PL	LIPe	-0.268	0.660
	LIPi	-0.023	0.568
	VIP	0.793	0.507
	PIP#1	-0.268	0.000
TL	CITv	0.466	0.560
	TEm	-0.350	0.691
	PITd	-0.023	0.142
	PITv	0.058	0.500
	IPa	0.385	0.710
	MT	2.997	0.314
	FST	1.446	0.454
	MSTp	0.140	0.231
	MSTd	1.446	0.497
OL	V3A	0.793	0.159
	V3v	0.711	0.000
	V4t	0.140	0.338
	DLr	-0.921	0.000
	DLc	-0.921	0.000
	V4v	-0.758	0.000
	VPP	-0.921	0.000
	V6	1.283	0.447
	DP	0.303	0.443
	VOT	-0.595	0.000
	V1	1.283	0.250
	V2	3.160	0.387
	Thal	LGN	-0.595
PII-s		-0.921	0.000
PIp		-0.840	0.000
PIm		-0.513	0.245
PII		-0.431	0.000
PIc		-0.431	0.219
PLa#1		-0.921	0.000
PLvl		-0.758	0.000
PLvm		-0.758	0.000
BG	Cd.g	-0.105	0.653
MB	MB#2	-0.187	0.298

2.2 Modular decomposition of the cortical and sub-cortical subdivisions of the Macaque brain

As mentioned in the main text, there is no simple correspondence between the modules and the anatomical subdivisions of the brain. The nodes of the connectome we have investigated are brain regions that belong to larger subdivisions, such as the prefrontal cortex, which in turn are part of broader anatomical categories such as the frontal lobe. The association between the network modules and the largest subdivisions have been shown in Fig. 1(d) in the main text. A more detailed representation of this relation is given in terms of the modular spectra of the anatomical subdivisions in Table S2 which indicates how the regions belonging to each subdivision are distributed among the five modules. We note that some of the subdivisions constitute a single brain region in the connectome we consider (e.g., Visual area V1 in the Occipital lobe), so that they belong exclusively to one of the modules. Larger subdivisions that comprise multiple regions, on the other hand, can have their constituent regions distributed non-uniformly among several modules. In such cases, we highlight the dominant module(s) of the subdivision, i.e., those amongst the five modules having the largest number of brain regions, in the table. The spatial layout of the brain regions belonging to these larger subdivisions, colored according to the modules to which they belong, are also shown in Figs. S5 and S6. Note that, the regions belonging to the parietal lobe occur predominantly in module #2, while those in the occipital lobe occur predominantly in module #5 (see Fig. S5). Fig. S6 suggests that the regions belonging to the basal ganglia mostly occur in module #3.

Table S2: Modular decomposition of the brain regions in different anatomical subdivisions of the Macaque brain.

Lobe/Nuclei (no. of brain regions)	Subdivision [abbreviation]	modular distrib.				
		1	2	3	4	5
Frontal lobe (58)	beltline of sensorymotor syst. [belt_sm]	0	1	0	0	0
	Prefrontal cortex [PFC]	18	5	0	11	2
	Supplementary motor area [Area 6]	3	11	1	0	0
	Primary motor area [MI]	0	4	2	0	0
Temporal lobe (56)	Ventral temporal cortex [TCV]	4	0	6	0	0
	Parahippocampal cortex [PHC]	3	0	11	0	0
	Hippocampus [Hip]	0	0	3	0	0
	Superior temporal gyrus [STG]	0	0	0	11	0
	Inferotemporal area [TE]	0	0	3	0	4
	Superior temporal sulcus [STS]	0	1	0	5	5
Parietal lobe (27)	Primary somatosensory cortex [S1]	0	4	0	0	0
	Secondary somatosensory cortex [S2]	0	1	1	0	0
	beltline of sensory syst. [belt_s]	1	0	0	0	0
	Rostral parietal area [PR#4]	0	1	0	0	0
	Somatosensory association area [7#1]	0	5	0	2	0
	Cortex of intraparietal sulcus [PCip]	0	2	0	0	4
	Dorsal parietal cortex [PCd#2]	0	6	0	0	0
Occipital lobe (16)	Visual anterior cortex [VAC]	0	1	0	0	12
	Visual area V1 [V1]	0	0	0	0	1
	Prostriate cortex [ProST]	1	0	0	0	0
	Visual area V2 [V2]	0	0	0	0	1
Thalamus (53)	Anterior nuclei [AN]	2	1	0	0	1
	Midline nuclei [ML]	5	1	1	0	0
	Geniculate nucleus [GN]	0	0	0	1	1
	Intralaminar nuclei [IL2]	1	3	0	1	0
	Massa intermedia [MI1]	0	1	0	0	0
	Posterior nuclei [PN]	0	0	0	2	0

	Reticularis thalami [Ret]	0	1	0	0	0
	Pulvinaris thalami [Pul#1]	0	1	0	3	8
	Medial dorsal nucleus [MD]	3	2	0	1	0
	Ventrolateral nuclei [VN]	1	12	0	0	0
Basal Ganglia (31)	Amygdala [Amyg]	0	0	22	0	0
	Substantia nigra [SN]	0	0	1	0	0
	Substantia innominata [SI#2]	1	0	0	0	0
	Nucleus subthalamus [Sub.Th]	0	0	1	0	0
	Globus pallidus [GPe]	0	0	0	0	1
	Striatum [STR]	1	1	1	0	1
	Clastrum [Clau]	0	1	0	0	0
Cingulate Gyrus (13)	Area 24 [24]	3	1	0	0	0
	Area 23 [23]	2	2	0	0	0
	Area 26 [26]	0	0	2	2	0
	Area 25 [25]	0	0	1	0	0
Insula (9)	Granular insular cortex [Ig#1]	0	0	1	0	0
	Retroinsular cortex [Ri#1]	0	1	0	0	0
	Insular proisocortex [IPro]	0	1	0	0	0
	Parainsular field [Pi#1]	0	0	1	0	0
	Anterior insula [IA]	4	0	1	0	0
Hypothalamus (1)	Hypothalamus [Hyp]	0	0	1	0	0
Midbrain (1)	Midbrain [MB]	0	0	0	0	1
Olfactory complex (1)	Olfactory complex [OFC]	1	0	0	0	0

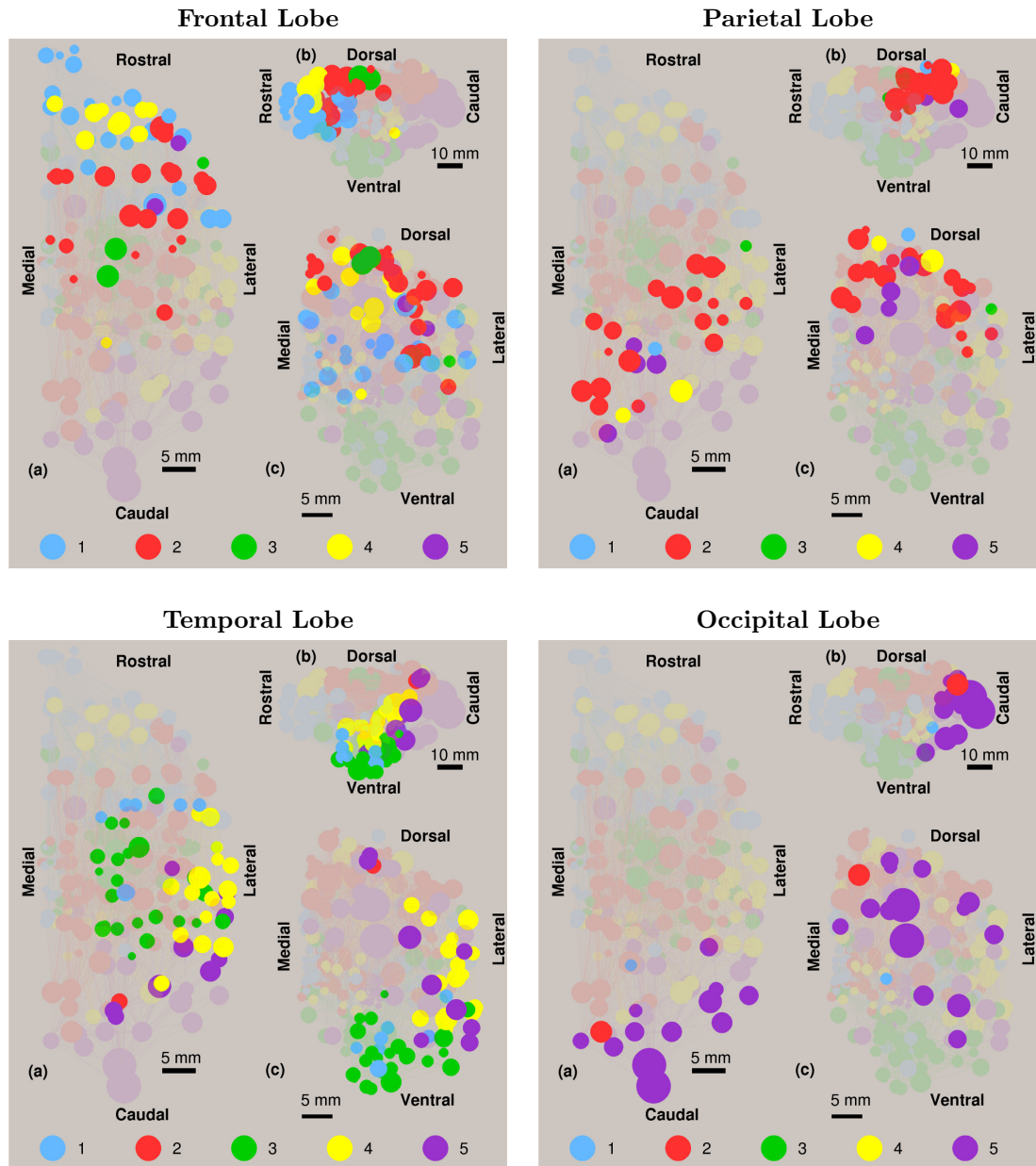


Figure S5: The network of brain regions shown in (a) horizontal, (b) sagittal and (c) coronal projections, indicating the modular memberships of the regions (highlighted) that belong to the frontal (top left), parietal (top right), temporal (bottom left) and occipital (bottom right) lobes. As in Fig. 1 (a-c) in the main text, the modular membership of each node is represented by its color (see color key at the bottom of each panel), the spatial positions of the nodes are specified by the three-dimensional stereotaxic coordinates of the corresponding regions, and node sizes provide a representation of the relative volumes of the corresponding brain regions (the spatial scale being indicated by the horizontal bar shown next to each projection).

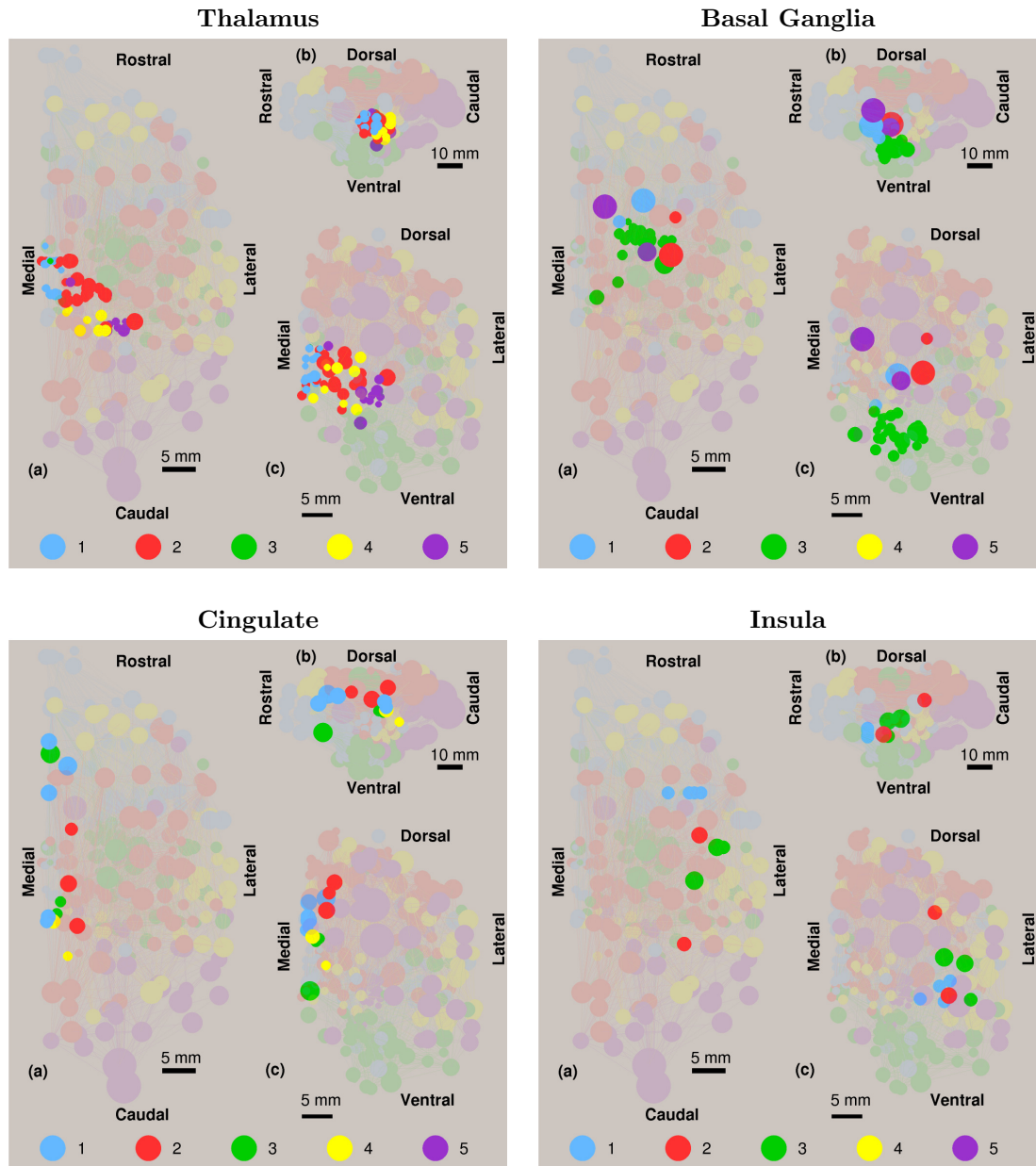


Figure S6: The network of brain regions shown in (a) horizontal, (b) sagittal and (c) coronal projections, indicating the modular memberships of the regions (highlighted) that belong to the thalamus (top left), basal ganglia (top right), cingulate (bottom left) and insula (bottom right). As in Fig. 1 (a-c) in the main text, the modular membership of each node is represented by its color (see color key at the bottom of each panel), the spatial positions of the nodes are specified by the three-dimensional stereotaxic coordinates of the corresponding regions, and node sizes provide a representation of the relative volumes of the corresponding brain regions (the spatial scale being indicated by the horizontal bar shown next to each projection).

2.3 Functional characterization of modules

As mentioned in the main text, we have investigated a possible structure-function correlation in the mesoscopic organization of the connectome, which would be reflected in the modules being predominantly associated with certain functionalities. In Table S3 we list the known functions (obtained from the literature) either of the brain regions belonging to each of the modules, or of the broader subdivisions to which such regions belong (the first column indicating the lobe or nuclei, and the second specifying the areas comprising it). As the different regions belonging to a subdivision may lie in distinct modules, the fraction of all the regions in a subdivision that are in a specific module are indicated in the third column. The role that these regions play in terms intra- and inter-modular communication can be inferred from the average values (computed over all the regions in the subdivision that are in the same module) of the participation coefficient, $\langle p \rangle$, and the within-module degree z -score, $\langle z \rangle$, which are shown in the fourth and fifth columns, respectively. Some of the brain regions in a subdivision that have been investigated relatively more extensively are mentioned in the sixth column, while the seventh column provides a non-exhaustive list of the functions that are known to be associated with these regions and/or the subdivision to which they belong (along with references to the relevant literature). As alluded to in the main text, regions belonging to the same module have certain functions that appear to complement each other in carrying out a specific cognitive task, e.g., high-level multimodal sensory integration and decision-making (module #1), motor control and somato-sensory processing (module #2), memory and emotion (module #3), auditory processing (module #4) and visual processing (module #5).

Table S3: Functional characterization of modules

Module #1						
Lobe/Nuclei	Subdi- vision	Frac.	$\langle p \rangle$	$\langle z \rangle$	Notable regions	Known functions
Frontal lobe	PFC	18/36	0.24	0.63	10, 11, 13, 14	sensory integration, decision making [7, 8, 9, 10, 11]
	Area 6	3/15	0.48	-0.18	6Va, 6Vb, PrCo	complex locomotion (e.g. climbing) [12, 13]
Temporal lobe	TCv	4/10	0.00	-0.51		
	PHC	3/14	0.17	-0.68	EO	olfaction [14]
Parietal lobe	belt_s	1/1	0.64	-0.70		
Occipital lobe	ProSt	1/1	0.50	-0.86		
Thalamus	AN	2/4	0.52	-0.62		
	ML	5/7	0.39	-0.78		
	IL#2	1/5	0.00	-0.90		
	MD	3/6	0.00	-0.75		
	VN	1/12	0.57	-0.15		
Basal Ganglia	SI#2	1/1	0.41	0.22		
	STR	1/4	0.43	0.22	Pu_r	motor skills, reinforcement learning [15]
Cingulate gyrus	Area 24	3/4	0.57	0.60	24a, 24b, 24c	emotional behavioural control [16]
	Area 23	2/4	0.61	-0.55	23a,23b	multi-sensory integration [16]
Insula	IA	4/5	0.33	0.70	Iam, Iai	social cognition [17]
olfactory complex	OFC	1/1	0.40	-0.68		olfaction [14]

Module #2						
Lobe/nuclei	Subdi- vision	Frac.	$\langle p \rangle$	$\langle z \rangle$	Notable regions	Known function
Frontal lobe	belt_sm	1/1	0.54	-0.52		
	PFC	5/36	0.48	-0.46	45B, 8Ad	saccadic guidance (frontal eye field) [18]
	Area 6	11/15	0.36	0.66		complex locomotion (climbing etc.) [12]
	MI	4/6	0.27	0.20	M1-FL, M1-HL	voluntary movement (primary motor area) [19]
Temporal lobe	STS	1/11	0.44	-0.98		
Parietal lobe	S1	4/4	0.21	0.46		primary somatosensory cortex [19]
	S2	1/2	0.00	-0.92	SII-f	secondary somatosensory area (face representation) [20]
	PR#4	1/1	0.00	-0.69		
	Area 7	5/7	0.10	-0.28	PF#1, PFG#1	visual-motor coordination [21]
	PCip	2/6	0.24	0.12	AIP, MIP	visual control of reaching & pointing [22, 23]
	PCd#2	6/6	0.39	0.91	PEm, PEc#1	somesthesia & motor control [24]
Occipital lobe	VAC	1/13	0.38	0.23		
Thalamus	AN	1/4	0.72	-0.86		
	ML	1/7	0.59	-0.63		
	IL#2	3/5	0.50	0.07		
	MI#1	1/1	0.00	-1.09		
	Ret	1/1	0.34	-0.29		
	Pul#1	1/12	0.29	0.58		
	MD	2/6	0.60	-0.50		
	VN	12/13	0.19	-0.45		somatosensory information relay [19]
Basal Ganglia	STR	1/4	0.37	-0.50	Pu.c	motor skills, reinforcement learning [15]
Cingulate gyrus	Area 24	1/4	0.29	-0.11		
	Area 23	2/4	0.46	1.06		
Insula	Ri#1	1/1	0.49	-0.63		
	Ipro	1/1	0.00	-1.03		
Module #3						
Lobe/nuclei	Subdi- vision	Frac.	$\langle p \rangle$	$\langle z \rangle$	Notable regions	Known function
Temporal lobe	TCv	6/10	0.16	0.82	35, 36c, 36r	visual perception & memory of objects [25]

	PHC	11/14	0.46	0.09	TH	spatial memory [26]
	Hip	3/3	0.28	-0.38		spatial cognition [27, 28] and recognition memory [29]
	TE	3/8	0.65	0.17		
Parietal lobe	S2	1/2	0.50	-1.16		
Basal Ganglia	Amyg	22/22	0.20	0.1		emotional response [30, 31]
	SN	1/1	0.61	-0.88		
	STR	1/4	0.57	-0.80	Cd.t	reinforcement learning [15]
Cingulate gyrus	Area 26	2/2	0.57	-0.88		
	Area 25	1/1	0.65	2.48		
Insula	Ig#1	1/1	0.60	0.83		
	Pi#1	1/1	0.64	0.19		
	IA	1/5	0.70	0.90		
Hypothalamus	Hyp	1/1	0.69	-0.80		
Module #4						
Lobe/nuclei	Subdivision	Frac.	$\langle p \rangle$	$\langle z \rangle$	Notable region	Known function
Frontal lobe	PFC	11/36	0.55	0.25	46d, 46v	working memory [32, 33]
Temporal lobe	STG	11/11	0.39	0.17	A1	auditory cortex [34, 35]
	STS	5/11	0.52	-0.04	TPOc, TAa, Pga	complex sound processing [36, 35]
Parietal lobe	Area 7	2/7	0.69	1.40	PG#1	somato-motor coordination [21]
Thalamus	GN	1/2	0.00	-0.53	MG	auditory information relay [19]
	IL#2	1/5	0.66	-0.67		
	PN	2/2	0.56	-0.08		
	Pul#1	3/12	0.00	-1.22		
	MD	1/6	0.66	-0.60		
Cingulate gyrus	Area 26	2/4	0.30	-0.81		
Module #5						
Lobe/nuclei	Subdivision	Frac.	$\langle p \rangle$	$\langle z \rangle$	Notable region	Known function
Frontal lobe	PFC	2/36	0.28	-0.30	45A, 8Ac	saccadic guidance (frontal eye field) [18]
Temporal lobe	TE	4/7	0.47	0.03	CITv, PITd, PITv, TEm	ventral visual pathway [37, 38]
	STS	5/11	0.44	1.28	MT, MST, FST	dorsal visual pathway [37, 38]
Parietal lobe	PCip	4/6	0.43	0.06	LIP, VIP, PIP	visual attention [39, 40]
Occipital lobe	VAC	12/13	0.11	-0.23	V3A, V3B, V6	visual cortex [19]

	V1	1/1	0.25	1.28		primary visual cortex [19]
	V2	1/1	0.39	3.15		secondary visual cortex [19]
Thalamus	AN	1/4	0.69	-0.51		
	GN	1/2	0.28	-0.59	LGN	visual information relay [19]
	Pul#1	8/12	0.06	-0.70		visual processing [41]
Basal Ganglia	Gpe	1/1	0.67	-0.84		
	STR	1/4	0.65	-0.10	Cd_g	reinforcement learning [15]
Mid brain	MB	1/1	0.30	-0.19		

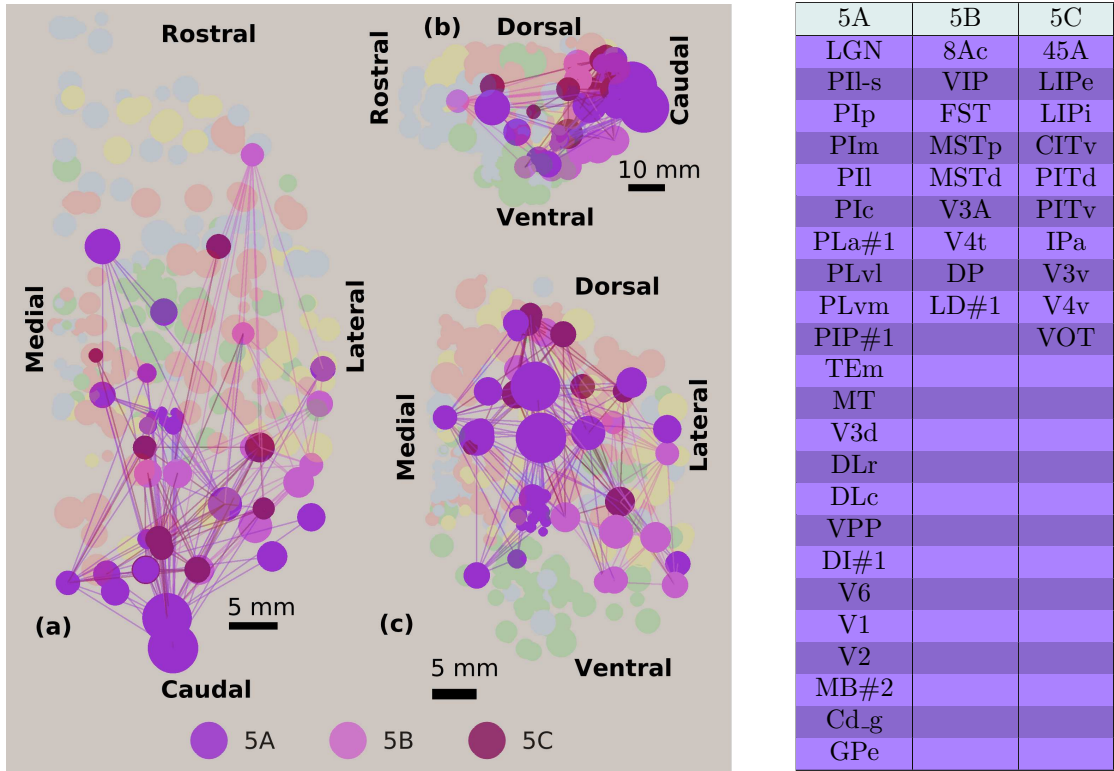


Figure S7: The network of brain regions shown in (a) horizontal, (b) sagittal and (c) coronal projections, indicating that the nodes in module #5 (highlighted) can be further grouped into three sub-modules. The sub-modular membership of each node of module #5 is represented by its color (see color key at the bottom) with the list of brain regions belonging to each of the three sub-modules shown in the table in the right. Sub-module #5A is seen to comprise primary visual regions and subcortical regions, while sub-modules #5B and #5C contain regions that belong to the ventral and dorsal visual pathways, respectively. The node sizes provide a representation of the relative volumes of the corresponding brain regions (the spatial scale being indicated by the horizontal bar in each panel). The spatial positions of the nodes are specified by the three-dimensional stereotaxic coordinates of the corresponding regions. Links indicate the directed nerve tracts connecting pairs of brain regions, and are colored in accordance with their source nodes.

The structure-function correlation associated with the mesoscopic organization, can be seen not only at the level of modules (as indicated by the Table reftab:tab3 above) but can be extended even further. As mentioned in the main text, we have subjected module #5 to further partitioning which yields three sub-modules. Fig. S7 shows the nodes in module #5 that belong to these sub-modules. We find that they are associated with distinct functionalities, with 5A containing the visual cortex and almost all the sub-cortical components, while the regions identified with different visual processing pathways, viz., the ventral and dorsal streams belong to 5B and 5C, respectively.

2.4 Categorization of nodes in terms of inter- intra-modular connectivity

As described in the main text, the role played by each of the brain regions in the mesoscopic organization of the connectome can be classified into seven categories according to their intra- and inter-modular connectivity, viz., R1: ultra-peripheral, R2: peripheral, R3: satellite connector, R4: kinless, R5: provincial hub, R6: connector hub, and R7: global hub (note that there are no regions in the Macaque brain belonging to the categories R4 and R7). With the exception of module #4 which has no region playing the role of a provincial hub, each module has a qualitatively similar distribution of its regions across these categories (Fig. S8, top).

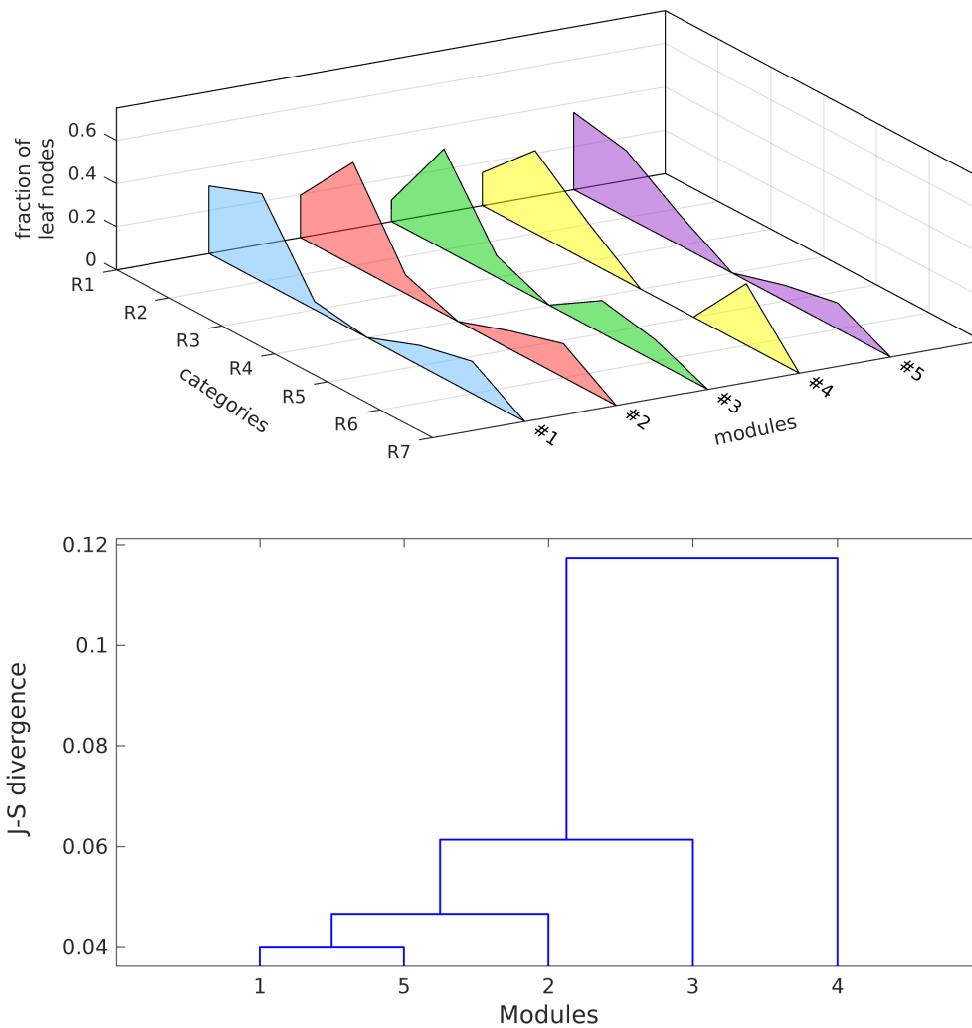


Figure S8: The distribution of the regions across the different categories R1-R7 (see Fig. 2 in main text) is similar for different modules (top), with the sole exception of module #4 which does not possess any provincial hub (R5) nodes. This is illustrated in the dendrogram (bottom) that represents the extent of similarity between these distributions, quantified by the Jensen-Shannon divergence, for the different modules.

The extent of similarity between the modules is represented by the dendrogram shown in Fig. S8 (bottom) in which the distance between the distributions across $x \in \{R1, \dots, R7\}$ for two

modules A and B , viz., $P_A(x)$ and $P_B(x)$, is measured in terms of the Jensen-Shannon divergence:

$$JSD(P_A, P_B) = \frac{1}{2} \sum_x \left[P_A(x) \ln P_A(x) + P_B(x) \ln P_B(x) - \{P_A(x) + P_B(x)\} \ln \left(\frac{P_A(x) + P_B(x)}{2} \right) \right].$$

This quantification of the difference between a pair of distributions is also employed in Fig. S9 to indicate the extent of similarity between the various anatomical subdivisions of the brain, the corresponding distributions of whose regions across the categories R1-R7 is shown in Fig. 2 (b) in the main text.

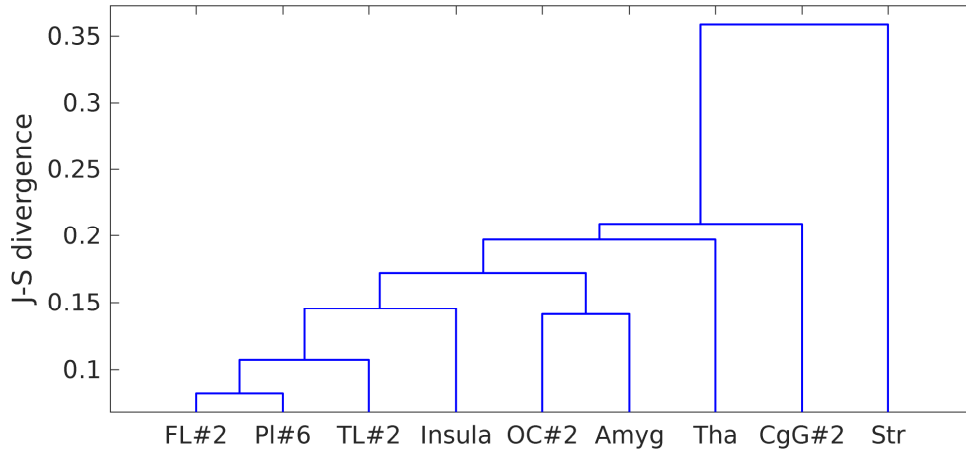


Figure S9: Dendrogram illustrating the extent of similarity between several anatomical subdivisions of the brain, viz., *Tha*: Thalamus, *FL#2*: Frontal Lobe, *Pl#6*: Parietal Lobe, *CgG#2*: Cingulate Gyrus, *Insula*, *TL#2*: Temporal Lobe, *OC#2*: Occipital Lobe, *Amyg*: Amygdala and *STR*: Striatum, in terms of the distribution across the categories R1-R7 of their constituent regions (see Fig. 2 (b) in main text). As in Fig. S8 (bottom), the difference between the distributions corresponding to two subdivisions is measured using the Jensen-Shannon divergence.

Next, we focus on how regions belonging to specific categories connect to each other. In the main text, we mention that within each module, the provincial hubs (R5) connect with each other significantly more often than expected by chance. This intra-modular connectivity between the R5 nodes can be clearly seen from Fig. S10, where these nodes are highlighted and their colors indicate the modules to which they belong (see color key at the bottom). Note that one of the projections shown here is identical to Fig. 2 (d).

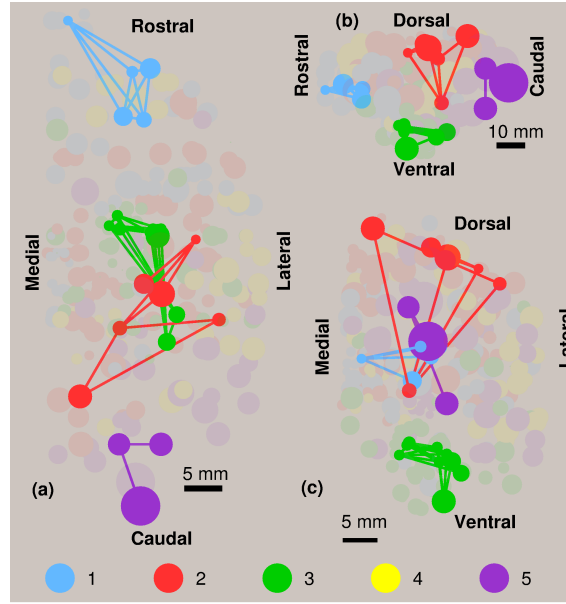


Figure S10: The network of brain regions in (a) horizontal, (b) sagittal and (c) coronal projections, showing that connections between provincial hubs (highlighted nodes) are localized within each module [Figure 2 (d) in the main text is identical to panel (b) above].

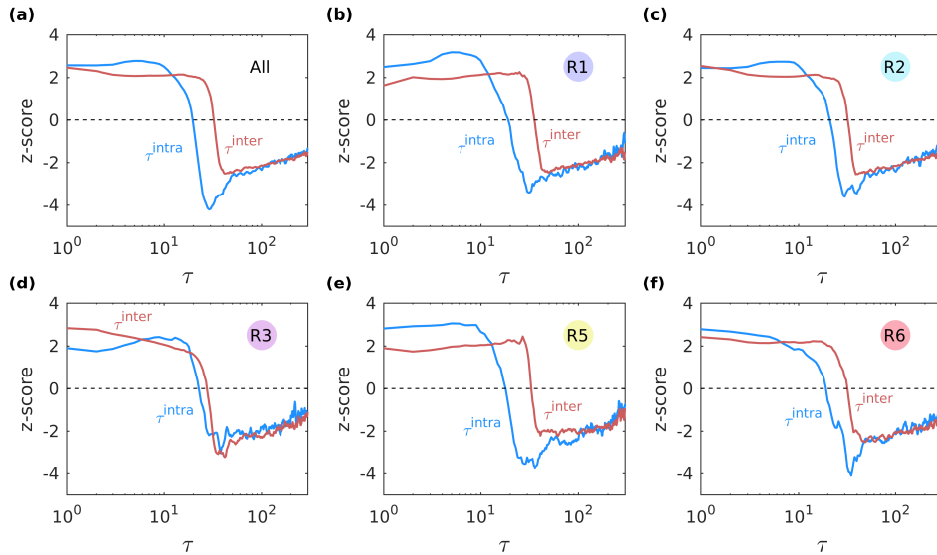


Figure S11: To see how the different categories R1-R7 of brain regions allow spreading to occur faster in the empirical brain network than in equivalent randomized networks, we compare the case where the source node can belong to any category (a) with those where the source is either ultra-peripheral R1 (b), peripheral R2 (c), satellite connector R3 (d), provincial hub R5 (e), or global hub R6 (f). The z -score indicates that there is a statistically significant shift in the empirical distribution towards lower values of τ in all cases. However, while for R3 the increase in the rate of spreading is similar irrespective of whether the target is in the same module or in a different one, we observe that there is a relatively larger shift at lower values for τ^{intra} as compared to τ^{inter} for most of the other categories (in particular, R1 and R5). Indeed, the latter behavior dominates when we consider sources across all categories [see panel (a)]. Note that panels (d) and (e) are identical to see Fig. 2 (g-h) in the main text.

In the main text we have described our investigation of the role played by regions belonging to different categories R1-R7 in facilitating information transmission. For this we simulate diffusive propagation within and between modules and obtain the distribution of first passage times for random walks between a source node and a target node. Fig. S11 (a) shows that the rate of diffusion in the connectome is enhanced both within a module and between modules (as indicated by the statistically significant shift - measured in terms of z -score - in the empirical distributions for both τ^{intra} and τ^{inter} towards lower values) as compared to that seen in equivalent randomized networks.

Fig. S11 (b-f) show how nodes belonging to categories R1, R2, R3, R5 and R6 (respectively), which have distinct intra- and inter-modular connectivity roles, contribute to enhancing communication in the connectome. In each case the source node belongs to the respective category and we quantify the difference in the distributions of both τ^{intra} and τ^{inter} from that obtained from randomized surrogates. We observe that for source nodes of most categories, with the exception of satellite connectors R3, the increase in the rate of diffusion within a module, compared to that in the surrogate networks, is even higher than the increase in the rate of diffusion across modules.

3 Spatial dependence of connectivity and modular organization

In the main text, we have stated that modular organization of the connectome is not primarily driven by constraints imposed by the physical distance between the brain regions. This is established by using three classes of surrogate random network ensembles to investigate how spatial embedding affects the modular decomposition of a network, with all the regions occupying the same positions in physical space as in the Macaque connectome. The three ensembles we have chosen for our investigation are specified by the dependence of the connection probability P between regions on the physical distance d between them, viz., (i) $P \sim d^0$, i.e., independent of the distance, (ii) $P \sim 1/d$, i.e., power-law dependence as in the empirical network, and (iii) $P \sim \exp(-d)$, i.e., exponential dependence, for which the constraint of distance most strongly affects the probability of connection. For each category, we have generated 100 different networks that have identical numbers of nodes and links as the empirical connectome. Subsequently, we subject these networks to community detection techniques using information about the connection topology alone, as well as space-independent modular decomposition which explicitly accounts for the dependence of P on d (see main text for details).

Fig. S12 shows how the modular nature of the networks belonging to each of the three ensembles described above vary upon two approaches for identifying the modules, viz., (i) using the topological information about the connections alone, and (ii) employing a space-independent partitioning that takes into account the dependence of the probability of connections between regions on the physical distance between them. The similarity between the modules obtained using these two methods is measured using normalized mutual information I_{norm} (see Methods in the main text). Note that, if the two types of partitionings yield identical modules then $I_{norm} = 1$, while $I_{norm} = 0$ implies maximal dissimilarity. Without any spatial dependence, the identified modules arise through fluctuations alone, and hence the similarity between the partitions obtained by the two methods will be entirely stochastic in nature, resulting in the broad distribution for I_{norm} seen in panel (a). In contrast, the ensemble underlying the distribution shown in panel (b) has an inverse relation between connection probability and physical distance, as in the empirical network. The value of I_{norm} obtained for the empirical network (indicated by the arrow) is seen to be significantly larger than those for the random ensemble. This suggests that had the modules arisen exclusively from a distance-dependent constraint on connections, the topological and space-independent approaches would have yielded highly dissimilar partitionings. Qualitatively similar results are obtained when the dependence of connection probability on physical distance is even stronger, viz., P decaying exponentially with d as in the case of the ensemble whose I_{norm} distribution is shown in panel (c). The fact that partitioning the empirical network using either

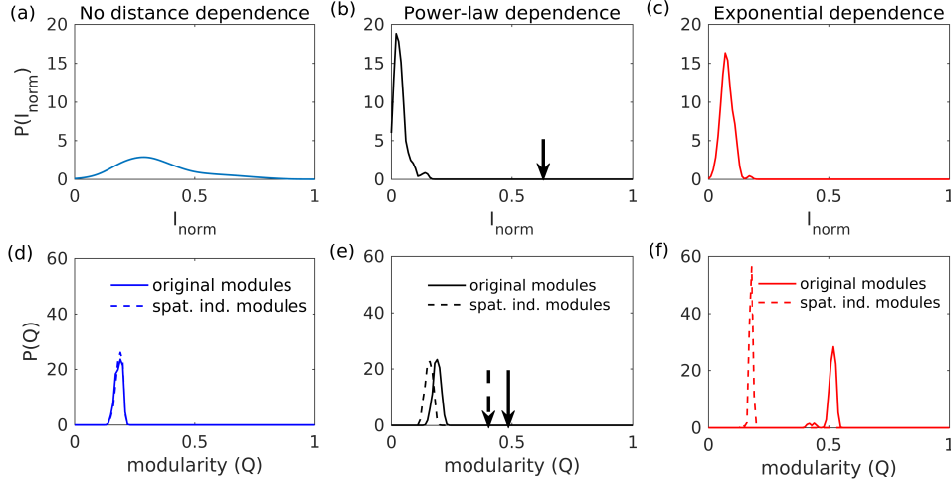


Figure S12: The distributions of (top row) the degree of similarity between the topological and space-independent modular partitionings of a network as measured by normalized mutual information I_{norm} between them, and (bottom row) the corresponding values for the modularity Q obtained using the two methods, for three types of random surrogate network ensembles. These are distinguished by the dependence of connection probability P between a pair of brain regions on the physical distance d between them, viz., $P \sim d^0$ [(a) and (d)], $P \sim 1/d$ [(b) and (e)] and $P \sim \exp(-d)$ [(c) and (f)]. As the Macaque connectome we have investigated also exhibits a power-law dependence, viz., $P \sim 1/d$, similar to that examined in (b) and (e), we have indicated in those panels the corresponding values for the empirical network (arrows).

the topological or the space-independent approach results in relatively similar modular decompositions suggest that constraints other than those related to physical distance plays a significant role in shaping the mesoscopic organization of the Macaque connectome. The results described above are supported by the corresponding distributions of the modularity Q measured for the different partitionings obtained using each of the two approaches (broken and solid curves in panels d-f). Thus, in the absence of any spatial dependence, the distributions of Q obtained using the topological and the space-independent approaches completely overlap [as seen in (d)]. When $P \sim d^{-1}$, the relatively weak spatial dependence gives rise to marginally lower values of Q for the partitionings obtained using the space-independent method, as compared to those obtained using the topological information alone. This is seen to be true for both the empirical network (broken and solid arrows) and the random ensembles [panel (e)]. With the stronger spatial dependence inherent in an exponentially decaying functional relation, we expect to see much larger differences in the Q values for the two types of partitionings, and this is indeed observed in the distributions shown in panel (f). Therefore, the more dominant the role of the constraint on physical distance in determining the connections, the more dissimilar the partitionings obtained by the two methods and the larger the difference in the corresponding Q values.

Fig. S13 illustrates the space independent modular organization of random networks with the three different types of spatial constraints as described above, employing the representation used in Fig. 3. The distributions of the physical distances d between the nodes and the nature of variation of the connection probability between nodes with d are shown in the panels (a) for networks the role of spatial constraint on connectivity is (left) absent, viz., $P \sim d^0$, (center) weak, viz., $P \sim 1/d$, and (right) strong, viz., $P \sim \exp(-d)$. Comparison of the modules obtained using the information about the connection topology alone and those determined using the space-independent method (shown in the panels (b) for each of the networks) indicate that in the absence of any dependence of P on d (left) the partitions overlap to a large extent. Introducing a role for the spatial constraint in determining the connections result in the two types of partitionings differing substantially. This is seen for the power-law dependence of P on d (center), but most prominently when P decays

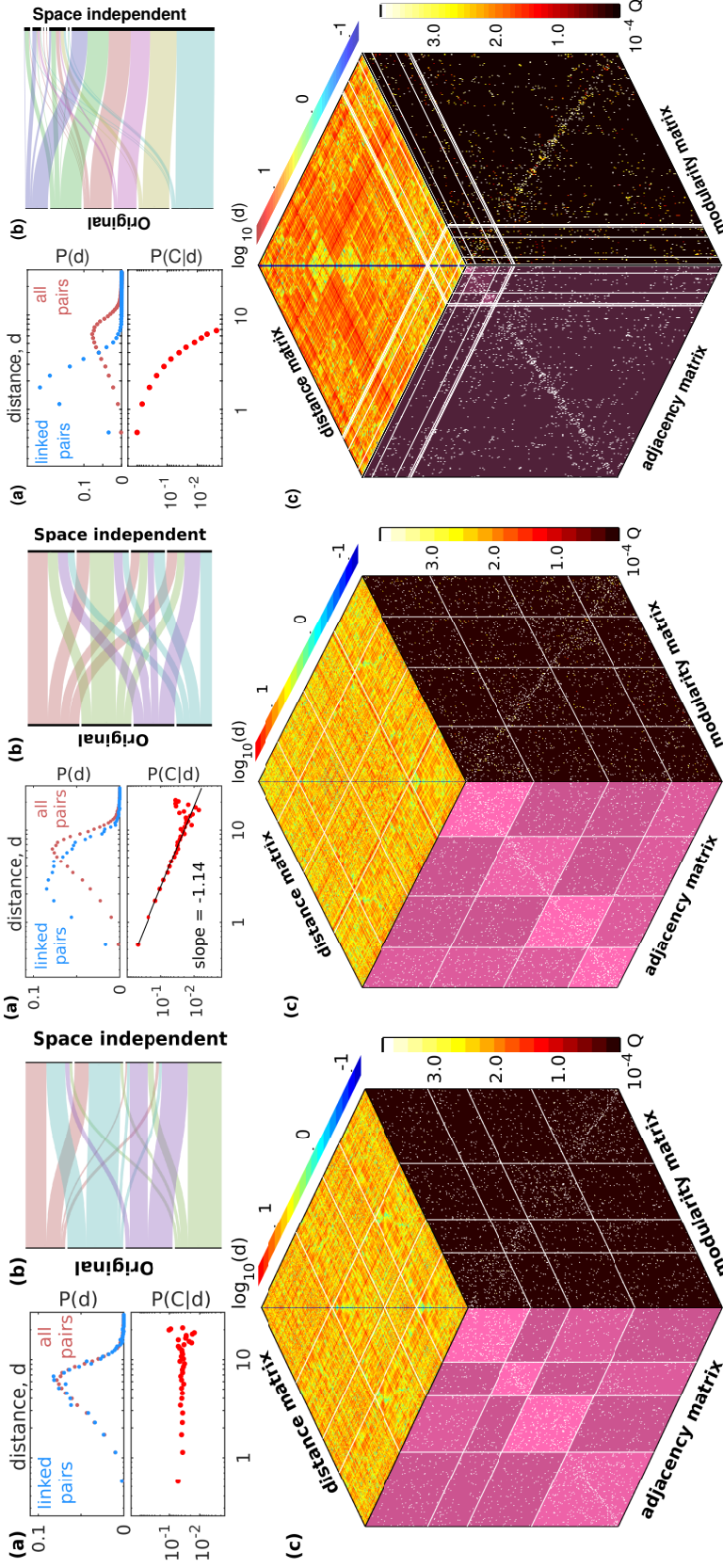


Figure S13: The dependence of the modular organization of a network on the three-dimensional spatial arrangement of the nodes shown for three different functional relations between the physical distance d between a pair of nodes and the connection probability P between them, viz., (left) $P \sim d^0$, (center) $P \sim 1/d$, and (right) $P \sim \exp(-d)$. For each functional relation, we show (a, top) the probability distribution of the physical distances d between all pairs of nodes (red) contrasted with that of the connected pairs (blue), as well as (a, bottom) the variation of the connection probability $P(C|d)$ with physical distance d which characterizes the functional relation (the best fit power-law is indicated with a line, along with its slope, in the central panel). The panels also contain (b) visual representations of the correspondence between the network modules determined using exclusively information about the connection topology (“Original”) and those obtained from space-independent partitioning of the network into communities. on the right). This alluvial diagram has been created using the online visualization tool RAW [4]. Joint representation of the space-independent modular organization of each class of network is shown in (c) using three matrices indicating adjacency $\{A_{ij}\}$ (left surface), modularity $\{B_{ij}\}$ (normalized by total number of links L , right surface) and physical distance $\{d_{ij}\}$ (top surface). As in Fig. 3 (b) of the main text, the nodes are grouped into partitions corresponding to the space-independent modules of the network with the boundaries indicated by solid lines.

exponentially with d (right). For the latter case, a single large module is seen to encompass the bulk of the network. As in this case the topological modules arise primarily from the spatial constraint on connections between nodes, on taking this dependence on d into account in the space-independent method the mesoscopic structure becomes relatively homogeneous. The panels (c) show the joint representation of the adjacency, modularity and physical distance matrices for each of the the three networks [as per the convention used in Fig. 3 (b) of the main text]. The partitions obtained by using the space-independent method are indicated by bounding lines in each matrix. Note that when we take into account the constraint that physical distance places on connectivity between regions, the partitioning results in modules that exhibit only a marginally higher density of connections within them (compared to the overall connection density). This is expected as the modules observed in the topological arrangement of connections in these random networks arise exclusively from the spatial constraint, and therefore the space-independent method should render the networks relatively homogeneous. Thus, the observation of non-trivial modules in the empirical network upon partitioning it with the space-independent method suggests that the observed mesoscopic organization of the Macaque connectome cannot be explained exclusively by the spatial layout of the regions.

References

- [1] Modha DS, Singh R (2010) Network architecture of the long-distance pathways in the macaque brain. *Proc Natl Acad Sci USA* 107(30):13485–13490.
- [2] Rosvall M, Bergstrom CT (2008) Maps of random walks on complex networks reveal community structure. *Proc Natl Acad Sci USA* 105(4):1118–1123.
- [3] Newman MEJ (2006) Modularity and community structure in networks. *Proc Natl Acad Sci USA* 103(23):8577–8582.
- [4] Mauri M, Elli T, Caviglia G, Uboldi G, Azzi M (2017) Rawgraphs: A visualisation platform to create open outputs in *Proceedings of the 12th Biannual Conference on Italian SIGCHI Chapter*, CHIItaly '17. (ACM, New York, NY, USA), pp. 28:1–28:5.
- [5] Good BH, De Montjoye YA, Clauset A (2010) Performance of modularity maximization in practical contexts. *Phys Rev E* 81(4):046106.
- [6] Lee JA, Verleysen M (2007) *Nonlinear dimensionality reduction*. (Springer Science & Business Media).
- [7] Walton ME, Behrens TEJ, Buckley MJ, Rudebeck PH, Rushworth MFS (2010) Separable learning systems in the macaque brain and the role of orbitofrontal cortex in contingent learning. *Neuron* 65(6):927–939.
- [8] Fellows LK (2007) The role of orbitofrontal cortex in decision making: a component process account. *Ann N Y Acad Sci* 1121(1):421–430.
- [9] Walton ME, Devlin JT, Rushworth MFS (2004) Interactions between decision making and performance monitoring within prefrontal cortex. *Nat Neurosci* 7(11):1259.
- [10] Izquierdo A, Suda RK, Murray EA (2004) Bilateral orbital prefrontal cortex lesions in rhesus monkeys disrupt choices guided by both reward value and reward contingency. *J Neurosci* 24(34):7540–7548.
- [11] Rolls ET (2000) The orbitofrontal cortex and reward. *Cereb Cortex* 10(3):284–294.
- [12] Graziano MS, Afalo TN (2007) Mapping behavioral repertoire onto the cortex. *Neuron* 56(2):239–251.

- [13] Gentilucci M, et al. (1988) Functional organization of inferior area 6 in the macaque monkey. *Exp Brain Res* 71(3):475–490.
- [14] Carmichael ST, Clugnet MC, Price JL (1994) Central olfactory connections in the macaque monkey. *J Comp Neurol* 346(3):403–434.
- [15] Apicella P, Ljungberg T, Scarnati E, Schultz W (1991) Responses to reward in monkey dorsal and ventral striatum. *Exp Brain Res* 85(3):491–500.
- [16] Baleyrier C, Mauguier F (1980) The duality of the cingulate gyrus in monkey. neuroanatomical study and functional hypothesis. *Brain* 103(3):525–554.
- [17] Evrard HC, Forro T, Logothetis NK (2012) Von Economo neurons in the anterior insula of the macaque monkey. *Neuron* 74(3):482–489.
- [18] Schall JD (2004) On the role of frontal eye field in guiding attention and saccades. *Vis Res* 44(12):1453–1467.
- [19] Kandel E, Schwartz J, Jessell T (2000) *Principles of Neural Science, Fourth Edition*. (McGraw-hill, New York) Vol. 4.
- [20] Manzoni T, Conti F, Fabri M (1986) Callosal projections from area sII to sI in monkeys: anatomical organization and comparison with association projections. *J Comp Neurol* 252(2):245–263.
- [21] Andersen RA, Asanuma C, Essick G, Siegel R (1990) Corticocortical connections of anatomically and physiologically defined subdivisions within the inferior parietal lobule. *Journal of Comparative Neurology* 296(1):65–113.
- [22] Sakata H, Taira M, Murata A, Mine S (1995) Neural mechanisms of visual guidance of hand action in the parietal cortex of the monkey. *Cereb Cortex* 5(5):429–438.
- [23] Eskandar EN, Assad JA (1999) Dissociation of visual, motor and predictive signals in parietal cortex during visual guidance. *Nat Neurosci* 2(1):88–93.
- [24] Caminiti R, Ferraina S, Johnson PB (1996) The sources of visual information to the primate frontal lobe: a novel role for the superior parietal lobule. *Cereb Cortex* 6(3):319–328.
- [25] Murray EA, Bussey TJ, Saksida LM (2007) Visual perception and memory: a new view of medial temporal lobe function in primates and rodents. *Annu Rev Neurosci* 30:99–122.
- [26] Malkova L, Mishkin M (2003) One-trial memory for object-place associations after separate lesions of hippocampus and posterior parahippocampal region in the monkey. *J Neurosci* 23(5):1956–1965.
- [27] Matsumura N, et al. (1999) Spatial- and task-dependent neuronal responses during real and virtual translocation in the monkey hippocampal formation. *J Neurosci* 19(6):2381–2393.
- [28] Courellis HS, et al. (2019) Spatial encoding in primate hippocampus during free navigation. *PLoS Biol* 17(12).
- [29] Jutras MJ, Buffalo EA (2010) Recognition memory signals in the macaque hippocampus. *Proc Natl Acad Sci USA* 107(1):401–406.
- [30] Weiskrantz L (1956) Behavioral changes associated with ablation of the amygdaloid complex in monkeys. *J. Comp. Physiol. Psychol.* 49(4):381.
- [31] Davis M (1992) The role of the amygdala in fear and anxiety. *Annu Rev Neurosci* 15(1):353–375.

- [32] Petrides M (1991) Monitoring of selections of visual stimuli and the primate frontal cortex. *Proc R Soc Lond, Ser B* 246(1317):293–298.
- [33] Petrides M (1995) Impairments on nonspatial self-ordered and externally ordered working memory tasks after lesions of the mid-dorsal part of the lateral frontal cortex in the monkey. *J Neurosci* 15(1):359–375.
- [34] Morel A, Garraghty P, Kaas J (1993) Tonotopic organization, architectonic fields, and connections of auditory cortex in macaque monkeys. *J Comp Neurol* 335(3):437–459.
- [35] Romanski LM, Averbeck BB (2009) The primate cortical auditory system and neural representation of conspecific vocalizations. *Annu Rev Neurosci* 32:315–346.
- [36] Barraclough NE, Xiao D, Baker CI, Oram MW, Perrett DI (2005) Integration of visual and auditory information by superior temporal sulcus neurons responsive to the sight of actions. *J Cogn Neurosci* 17(3):377–391.
- [37] Goodale MA, Milner AD (1992) Separate visual pathways for perception and action. *Trends Neurosci* 15(1):20–25.
- [38] Goodale MA, Milner AD (2018) Two visual pathways where have they taken us and where will they lead in future? *Cortex* 98:283–292.
- [39] Duhamel JR, Colby CL, Goldberg ME (1998) Ventral intraparietal area of the macaque: congruent visual and somatic response properties. *J Neurophysiol* 79(1):126–136.
- [40] Pesaran B, Pezaris JS, Sahani M, Mitra PP, Andersen RA (2002) Temporal structure in neuronal activity during working memory in macaque parietal cortex. *Nat Neurosci* 5(8):805–811.
- [41] Smelser NJ, Baltes PB (2001) *International encyclopedia of the social & behavioral sciences*. (Elsevier Amsterdam) Vol. 11.